Discovery of the late autophagy inhibitor FZU-0045-053 and its anti-breast cancer and immunomodulatory effects

JINLAN LUO[1,2*], YI YANG[1,3*], LULU CHENG[1,3*], FANGTING CHENG[1,3], HUANGWENLONG ZHUANG[3], SHANSHAN CHEN[1], PANPAN QIAO[4], YINBIN LIANG[1,2,5], LI CHEN[3], YANG SUN[1,2,5], HAIJUN CHEN[4] and QINYING LIU[1,5]

[1]Fujian Provincial Key Laboratory of Tumor Biotherapy, Clinical Oncology School of Fujian Medical University, Fujian Cancer Hospital, Fuzhou, Fujian 350014, P.R. China; [2]Department of Gynecology, Clinical Oncology School of Fujian Medical University, Fujian Cancer Hospital, Fuzhou, Fujian 350014, P.R. China; [3]Fujian Provincial Key Laboratory of Medical Instrument and Pharmaceutical Technology, College of Biological Science and Technology, Fuzhou University, Fuzhou, Fujian 350108, P.R. China; [4]Key Laboratory of Molecule Synthesis and Function Discovery, College of Chemistry, Fuzhou University, Fuzhou, Fujian 350108, P.R. China; [5]Interdisciplinary Institute for Medical Engineering, Fuzhou University, Fuzhou, Fujian 350108, P.R. China

Received May 13, 2025; Accepted September 29, 2025

DOI: 10.3892/ijo.2025.5823

Abstract. Breast cancer is characterized by notable heterogeneity and remains one of the leading causes of cancer-related death among women. Autophagy, a process by which cells use lysosomes to degrade cytoplasmic proteins and damaged organelles, is not only associated with chemotherapy resistance, but is also involved in immune-mediated tumor cell killing and immune evasion, making it a promising target for cancer therapy. Pharmacological inhibition of autophagy in breast cancer cells suppresses tumor progression. In the present study, the small molecular compound FZU-0045-053 (053) was identified, which exhibited autophagic and immunomodulatory effects. The effect of 053 on autophagy regulation in breast cancer cells was evaluated using transmission electron microscopy, an mRFP-GFP- microtubule-associated protein 1 light chain 3 (LC3) tandem fluorescent adenovirus, the CYTO-ID Autophagy Detection Kit and western blot analysis. Cell viability was subsequently assessed with proliferation assay and ATP assay kits. Apoptosis induction and the expression of immune-related molecules were measured by flow cytometry. Furthermore, a triple-negative breast cancer mouse model was established to validate the antitumor and autophagy-modulating effects of 053 *in vivo* using immunofluorescence and immunohistochemical staining. Finally, a 4T1 syngeneic mouse model was utilized to corroborate the immunomodulatory effects of 053 *in vivo* through immunohistochemistry and flow cytometric analysis. The findings indicated that 053 regulated autophagy in the breast cancer cell lines MDA-MB-231 and MCF-7, similar to the late autophagy inhibitor chloroquine. This regulation resulted in the accumulation of autophagic substrates, specifically LC3-II and sequestosome 1, by blocking autophagic flux. By blocking autophagy flux, 053 suppressed proliferation, induced apoptosis and ultimately restored chemosensitivity in MDA-MB-231 cells. In addition, the MDA-MB-231 xenograft model indicated that 053 inhibited autophagy by blocking autophagic flux, which lead to the accumulation of LC3 and sequestosome 1. 053 also negatively regulated the expression of programmed death-ligand 1 (PD-L1) in tumor cells. The 4T1 xenograft model showed that 053 had a notable immune-promoting effect, whereby it not only negatively regulated the expression of PD-L1 in tumor cells but also modulated T cell activation and proliferation by downregulating the expression of co-inhibitory molecules (T-cell immunoglobulin and mucin-domain containing-3 and programmed cell death protein 1) on T cells and upregulating co-stimulatory molecules (4-1BB, OX40 and inducible T-cell co-stimulator). *In vivo* xenograft models demonstrated that 053 had notable antitumor effects and high biosafety, with improved antitumor efficacy when combined with the chemotherapy drug gemcitabine. In summary, 053 can block autophagy and promote antitumor immune responses, showing promise as a new generation of adjuvant drugs for tumor chemotherapy and immunotherapy.

Correspondence to: Dr Qinying Liu, Fujian Provincial Key Laboratory of Tumor Biotherapy, Clinical Oncology School of Fujian Medical University, Fujian Cancer Hospital, 420 Fuma Road, Fuzhou, Fujian 350014, P.R. China
E-mail: liuqinyingbio@163.com

Dr Haijun Chen, Key Laboratory of Molecule Synthesis and Function Discovery, College of Chemistry, Fuzhou University, 2 Wulongjiang North Avenue, Fuzhou, Fujian 350108, P.R. China
E-mail: chenhaij@gmail.com

*Contributed equally

Key words: FZU-0045-053, breast cancer, autophagy inhibition, T cells

Introduction

Breast cancer is the most common malignant tumor among women worldwide (1). In clinical practice, immunohistochemical results are often used to define the four breast cancer subtypes, including luminal A, luminal B, human epidermal growth factor receptor 2 (HER2)-enriched and triple-negative breast cancer (TNBC) (2). Luminal A is characterized by high expression of the estrogen receptor (ER) and progesterone receptor (PR) as well as low expression of Ki67 and is HER2-negative, indicating slower cell growth and improved prognosis. Luminal B tumors are ER-positive and PR-positive, but they can be either HER2-positive or HER2-negative. They exhibit higher levels of Ki67, which indicates faster cell growth. HER2-enriched cancer is ER-negative and PR-negative and exhibits high Ki67 levels, indicating that the tumor is highly aggressive. TNBC lacks the expression of HER2, ER and PR, and is clinically recognized as the most therapeutically recalcitrant breast cancer subtype (3). Due to the notable invasiveness and high recurrence and metastasis rates of TNBC, chemotherapy resistance often develops during treatment, leading to a poor prognosis following conventional chemotherapy (4). Consequently, it is essential to further develop effective antitumor drugs with low toxicity that can reverse drug resistance.

Autophagy is a cellular biological process in which cells degrade dysfunctional organelles or unnecessary components through autophagosomes, subsequently recycling the nutrients for their growth (5). Previous research has identified autophagy as a promising therapeutic target in the treatment of cancer, and an increasing body of evidence supports that blocking autophagy can effectively inhibit the growth and progression of advanced tumors (6,7). In recent years, research has focused on targeting the various pathways involved in tumor progression, including the PI3K/AKT/mTOR and cyclin D/CDK/ retinoblastoma protein pathways (8,9). In this respect, autophagy inhibition has been demonstrated to enhance chemotherapeutic responsiveness.

Research indicates that metastatic cell lines have higher levels of basal autophagy compared with non-metastatic cell lines, suggesting that autophagy may enhance the invasiveness of tumor cells (10,11). High expression of microtubule-associated protein 1 light chain 3 (LC3) has been linked to tumor progression and poor outcomes in TNBC, demonstrating its potential as a prognostic biomarker for this disease (10). Furthermore, the knockout of autophagy-related genes, specifically LC3, has been shown to inhibit autophagy, leading to a marked decrease in cell proliferation, colony formation and migratory/invasive capabilities, while also promoting apoptosis in MDA-MB-231 cell lines (12). Overall, autophagy is essential for the survival of tumor cells (8). At present, the only autophagy inhibitors available for clinical application are chloroquine (CQ) and hydroxychloroquine (HCQ). However, these agents are associated with retinotoxicity and cardiotoxicity (13). Therefore, it is essential to further search for autophagy inhibitors with low toxicity that exhibit enhanced specificity.

Immune checkpoint molecules play a key role in the antitumor immune response. Cancer cells frequently exploit these mechanisms to evade immune surveillance, thereby facilitating cancer progression and contributing to treatment resistance (14). Immune checkpoint inhibitors regulate the TME through various mechanisms to exert their anticancer effects. With the development of cancer immunotherapy, targeting programmed cell death protein-1 (PD-1) or programmed death-ligand 1 (PD-L1) pathways can enhance antitumor immune activity and inhibit cancer cell proliferation (9). However, the low response rate of antitumor immunotherapy limits its efficacy (15). Furthermore, autophagy is a critical factor in tumor immunotherapy and interacts with immune cells to regulate therapeutic effects (16). Autophagy has been demonstrated to play a notable role in T cell activation and memory differentiation, and it can influence the immunogenicity of tumor cell death (17,18). In summary, cytoprotective autophagy and the immunosuppressive TME have been recognized as notable barriers. Consequently, the development of novel drugs that inhibit autophagy and possess immunomodulatory effects, or the use of multi-drug combinations, may further enhance therapeutic efficacy.

Inhibiting autophagy while modulating the antitumor immune response holds potential for effective tumor suppression. Small molecule compounds have demonstrated advantages for tumor-targeting therapy. These small molecule compounds can be easily modified to become more suitable for clinical needs, and their synthesis cost is low and easy to promote, which makes them hot spots in the current research of tumor-targeting therapy (9,19). LLY-507, a selective small-molecule inhibitor of SET and MYND domain-containing protein 2 (SMYD2), has been extensively validated for its mechanism of action and antitumor properties. LLY-507 exhibits submicromolar potency against SMYD2 in various cancer cell lines (such as esophageal squamous carcinoma, bladder carcinoma gastric cancer cell lines) by occupying the peptide-binding groove of SMYD2 (20-23). However, the impact of LLY-507 derivatives and their synthetic intermediates on tumor cell autophagy and immune modulation remains unexplored.

In the present study, a series of LLY-507 derivatives, including 26 intermediates, were screened. Through the mRFP-GFP-LC3 fluorescence tandem assay, CYTO-ID assay, monodansylcadaverine (MDC) staining and protein-level detection of LC3, the intermediate compound FZU-0045-053 (053) in the synthesis process of LLY-507 derivatives was preliminarily screened as having autophagy-regulating effects on breast cancer cells. To capture the spectrum of breast cancer heterogeneity, two representative cell lines were selected: MDA-MB-231 as a triple-negative ($ER^-/PR^-/HER2^-$) basal-like subtype and MCF-7 as a hormone receptor-positive (ER^+/PR^+) luminal subtype. This dual-model system provides a critical platform for mechanistic studies, drug discovery and personalized therapy development by encompassing both treatment-responsive and therapy-resistant phenotypes. At the cellular level, the effects of compound 053 on key autophagy markers were validated to elucidate its regulatory mechanism on autophagy in breast cancer cells. Apoptosis and proliferation assays were used to verify whether the combination of 053 and chemotherapy drugs could reverse chemotherapy resistance. The PD-L1 levels of tumor cells and the co-stimulatory or co-inhibitory molecules on the surface of T cells were detected to evaluate the effect of compound 053 on the immune response. Additionally, an MDA-MB-231 xenograft model was established to evaluate the antitumor and autophagy-regulating effects of 053± gemcitabine (GEM). The

4T1 xenograft model was established to assess the antitumor and immune-modulating effects of 053± GEM.

Materials and methods

Reagents. Compound 053 was dissolved in DMSO to prepare a 10 mM stock solution. CQ (cat. no. C129284) was purchased from Shanghai Aladdin Biochemical Technology Co., Ltd. and dissolved in DMSO to prepare a 10 mM stock solution. Rapamycin (RAPA; cat. no. HY-10219) was purchased from MedChemExpress and dissolved in DMSO to prepare a 10 mM stock solution. Adriamycin (ADM; cat. no. HY-15142A; MedChemExpress) was dissolved in DMSO to prepare a 10 mM stock solution. GEM (cat. no. HY-17026; MedChemExpress) was dissolved in DMSO to prepare a 100 mM stock solution. Paclitaxel (PTX; cat. no. HY-B0015; MedChemExpress) was dissolved in DMSO to prepare a 100 mM stock solution. Cisplatin (DDP; cat. no. HY-17394; MedChemExpress) was dissolved in DMSO to prepare a 100 mM stock solution. 5-Fluorouracil (5-FU; cat. no. HY-90006; MedChemExpress) was dissolved in DMSO to prepare a 100 mM stock solution.

Synthesis of compound 053. The synthesis, detailed synthetic procedure and characterization of compound 053 are described in Data S1.

Cells and cell culture. The breast cancer cell lines MCF-7 (cat. no. KGG3332-1), MDA-MB-231 (cat. no. KGG3220-1) and 4T1 (cat. no. KGG2224-1) (all from Nanjing Kaiji Biotechnology Co., Ltd.) were cultured in RPMI-1640 medium (cat. no. L210KJ; Shanghai Yuanpei Biotech Co., Ltd.) supplemented with 10% fetal bovine serum (FBS; cat. no. A0050-3110; Cegrogen Biotech GmbH) and 1% penicillin/streptomycin (cat. no. MA0110; Dalian Meilun Biology Technology Co., Ltd.).

Peripheral blood mononuclear cells (primary cells isolated from human blood) were obtained in accordance with the regulations established by The Ethics Committee of Fujian Provincial Cancer Hospital (Fuzhou, China; approval no. K2023-305-01) and with the informed consent of the participants. Blood samples were collected at the Fujian Provincial Key Laboratory of Tumor Biotherapy, Clinical Oncology School of Fujian Medical University, Fujian Cancer Hospital (Fuzhou, China). All participants were women, ranging in age from 25 to 40 years. The blood sample collection period extended from September 2023 to August 2024. Furthermore, the inclusion criteria for participants consisted of healthy adults without major diseases. CD3 (10 μg/ml; cat. no. T210; Takara Bio, Inc.) was used to coat 1 well of a 6-well plate overnight at 4˚C. A total of 4 ml peripheral blood was drawn from healthy individuals, and after removing the serum, it was diluted with PBS. The mixture was slowly added to a centrifuge tube containing 4 ml Ficoll Paque PREMIUM (cat. no. 17544202; Cytiva) and centrifuged at 800 x g with an acceleration of 8 and a deceleration of 0 for 20 min at room temperature. The middle white membrane layer was collected and washed twice with PBS. The cells were resuspended in X-VIVO 15™ culture medium (cat. no. 04-418Q; Lonza Group, Ltd.), which contained 10% FBS, 0.5 μg/ml interleukin-2 (cat. no. GMP-11848-HNAE; Beijing Sino Technology Co. Ltd.) and 0.25 μg/ml interferon-γ (IFN-γ; cat. no. 11725-HNAS; Beijing Sino Technology Co. Ltd.). The cell mixture was transferred to the CD3-coated plate, and 25 μl/ml CD3/CD28 (cat. no. 10971; Stemcell Technologies, Inc.) was added. The cell culture conditions were a constant temperature of 37˚C and a gaseous environment of 5% CO_2.

mRFP-GFP-LC3 fluorescence tandem assay. MCF-7 and MDA-MB-231 cells were transfected with the pGMLV-CMV-RFP-GFP-hLC3-Puro lentivirus (cat. no. GM-0220LV05-1; GemPharmatech Co., Ltd.) and were subsequently designated as MCF-7 GFP/RFP-LC3B and MDA-MB-231 GFP/RFP-LC3B, respectively. After adding viral supernatant at a multiplicity of infection (MOI) of 10 for MDA-MB-231 cells and MOI of 30 for MCF-7 cells, as well as 2 μg/ml polybrene (cat. no. C0351; Beyotime Biotechnology) for a co-incubation of 24 h, the medium was replaced with fresh complete medium. At 72 h post-viral transduction, 2 μg/ml puromycin was added to the cells and selection was continued for 2 weeks until all cells in the untransduced control group had died, after which subsequent experiments were conducted. Untransfected wild-type (WT) cells, MCF-7 WT and MDA-MB-231 WT, served as controls. As shown in Fig. S1A and B, after treatment with RAPA (10 μM) for 24 h to induce autophagy, clear red and green fluorescence signals were observed in the MCF-7 GFP/RFP-LC3B and MDA-MB-231 GFP/RFP-LC3B cells under fluorescence microscopy. By contrast, no significant fluorescence was detected in the control groups (MCF-7 WT and MDA-MB-231 WT). This demonstrated the successful establishment of stable cell lines expressing pGMLV-CMV-RFP-GFP-hLC3-Puro.

Next, MCF-7 GFP/RFP-LC3B or MDA-MB-231 GFP/RFP-LC3B cells (~1x10^4/well) were seeded into 24-well plates, which contained microscope cover glasses and cultured at 37˚C in a humidified atmosphere with 5% CO_2 for 24 h. Cells were then treated with 053 (5 μM), CQ (30 μM), RAPA (10 μM) or RAPA combined with CQ or 053 for 24 h. Microscope cover glasses containing cells were washed three times with PBS and fixed with 4% paraformaldehyde for 15 min at room temperature, washed three more times with PBS for 5 min each, air-dried and overlaid on slides dripped with DAPI anti-fluorescence attenuation sealer. The slides were observed and images were captured using an Olympus inverted fluorescence microscope (Olympus Corporation). The level of fluorescence was analyzed using ImageJ (1.8.0.1; National Institutes of Health) software.

CYTO-ID assay. MCF-7 or MDA-MB-231 cells (~5x10^4/well) were cultured in 24-well plates for 24 h, treated with RAPA (10 μM), CQ (30 μM) or 053 (0, 0.5, 2.5 or 5 μM) for 24 h and stained with CYTO-ID® Autophagy detection kit 2.0 (cat. no. ENZ-KIT175-0200; Enzo Life Sciences, Inc.). The CYTO-ID staining was observed and images were captured by inverted fluorescence microscope or detected by flow cytometry (MoFlo XDP; Beckman Coulter Ltd.). FlowJo software (v10.8.1; BD Biosciences) was used for analysis.

MDC staining. MCF-7 or MDA-MB-231 cells (~1x10^5/well) were seeded into 12-well plates and incubated overnight at 37˚C in a humidified atmosphere with 5% CO_2. Next, cells

were treated with 5 μM 053 and 30 or 60 μM CQ for 24 h. The cells were stained according to the MDC Staining Assay Kit (cat. no. C3018M; Beyotime Biotechnology) and detected by flow cytometry (MoFlo XDP). FlowJo software was used for analysis.

Brightfield microscopy. MCF-7 or MDA-MB-231 cells (~1x10^5/well) were seeded into 12-well plates and incubated overnight at 37˚C in a humidified atmosphere with 5% CO_2. Next, cells were treated with different concentrations of 053 (0, 2.5, 5, 10 or 20 μM) for 24 h. Micrographs were obtained using an inverted fluorescence microscope.

Transmission electron microscopy. MCF-7 or MDA-MB-231 cells (~1x10^5/well) were seeded into 12-well plates and incubated overnight at 37˚C in a humidified atmosphere with 5% CO_2. Next, cells were treated with 5 μM 053 for 24 h. The cells were collected, washed once with PBS and then resuspended in 2.5% glutaraldehyde and fixed at 4˚C for 24 h. After gradual dehydration with ethanol, the cells were treated with acetone for 10 min, followed by treatment with a mixture of epoxy resin and acetone. Finally, the samples were embedded in resin and subjected to ultrathin sectioning at a thickness of 60 nm. The sections were stained with uranyl acetate for 15 min at room temperature, washed twice with distilled water and subsequently stained with lead citrate for 5 min at room temperature. After a final thorough wash with ultrapure water, the samples were observed and imaged under the transmission electron microscope. Images were observed and captured using a FEI Tecnai 12 BioTwin transmission electron microscope (FEI; Thermo Fisher Scientific, Inc.).

Cell viability. MDA-MB-231 or 4T1 cells (~2x10^3/well) were seeded into 96-well plates and incubated for 24 h at 37˚C in a humidified atmosphere with 5% CO_2. After which, the cells were treated with 053 (0, 2.5, 5, 10 or 20 μM), 10 μM docetaxel (DOC), 50 μM DDP, 80 μM GEM, 0.1 μM PTX or 50 μM 5-fluoro-2,4-pyrimidinedione (5-FU) alone or combined with 053 (5 μM) for 24 h. The CellTiter 96® AQueous One Solution Cell Proliferation Assay (cat. no. G3581; Promega Corporation) was used to detect cell growth inhibition activity. Finally, the absorbance at 490 nm was measured using a microplate reader (Corona Electric Co., Ltd.). T cells (~2x10^3/well) were seeded into 96-well plates, and treated with 053 (0, 2.5, 5, 10 or 20 μM) for 24 h.

T cells were co-cultured with MDA-MB-231 cells at a 1:1 ratio, both of which were treated with 053 (0, 2.5, 5, 10 or 20 μM) for 24 h. The ATP Detection Assay Kit (cat. no. S0026; Beyotime Biotechnology) was used to evaluate T cell proliferation, and the relative light unit values were measured using a luminometer.

Western blotting. Western blot analysis was performed to evaluate the effects of compound 053, CQ or RAPA on the protein levels of LC3, p62, mTOR, phosphorylated (p-)mTOR, AKT and p-AKT. Western blot analysis was also conducted to assess the effects of compound 053, ADM, GEM and CQ on the protein levels of co-stimulatory and co-inhibitory molecules on the surface of T cells. Total proteins were extracted from cells with RIPA lysis buffer (cat. no. PC101; Shanghai Epizyme Biopharmaceutical Technology Co., Ltd.; Ipsen Pharma) and the BCA Protein Assay Kit (cat. no. P0012; Beyotime Biotechnology) was used for protein quantification. Equal amounts of protein (30 μg) were separated on a 12.5% SDS-PAGE gel (cat. no. PG113; Shanghai Epizyme Biopharmaceutical Technology Co., Ltd.; Ipsen Pharma) and transferred to a nitrocellulose transfer membrane (cat. no. 66485; Pall Corporation). The membrane was blocked by 5% w/v non-fat dry milk at room temperature for 1 h and incubated with the LC3B (cat. no. 83506; 1:1,000), p62 (cat. no. 88588; 1:1,000), AKT (cat. no. 4691; 1:1,000), p-AKT (cat. no. 9271; 1:1,000), p-mTOR (cat. no. 5536; 1:1,000), mTOR (cat. no. 2983; 1:1,000), T-cell immunoglobulin and mucin domain-containing protein 3 (TIM3; cat. no. 45208; 1:1,000), programmed cell death protein 1 (PD-1; cat. no. 86163; 1:1,000), V-domain immunoglobulin suppressor of T-cell activation (VISTA; cat. no. 54979; 1:1,000), CD40 ligand (CD40L; cat. no. 15094; 1:1,000) (all from Cell Signaling Technology, Inc.), tumor necrosis factor receptor superfamily, member 4 (OX40; cat. no. ab264466; 1:1,000; Abcam) and tumor necrosis factor receptor superfamily, member 9 (4-1BB; cat. no. ab68185; 1:1,000; Abcam) antibodies overnight at 4˚C. After washing the primary antibody away with 1X TBST (0.1% Tween-20), the membrane was incubated with the secondary antibody goat anti-mouse IgG (HRP conjugated; 1:10,000; cat. no. LF101; Shanghai Epizyme Biotech Co., Ltd.) or goat anti-rabbit IgG (HRP conjugated; 1:10,000; cat. no. LF102; Shanghai Epizyme Biotech Co., Ltd.) for 1 h at room temperature. The chemiluminescence detection was ultimately performed using a FluorChem E digital darkroom system (Bio-Techne).

Apoptosis assay. MDA-MB-231 cells (~1x10^5/well) were seeded into 12-well plates and incubated overnight at 37˚C in a humidified atmosphere with 5% CO_2. The commonly used concentrations of DOC in *in vitro* cell experiments range from 0 to 10 μM (24,25). Short-term high doses are used to observe rapid cytotoxicity or changes in signaling pathways. Experiments with sensitive cell lines (Luminal) typically use 50-100 nM, while invasive cell lines (TNBC) typically use 1-10 μM (26). Clinically, intravenous injections of 75-100 mg/m^2 DOC are administered, which require individualized adjustment. Clinical doses for the Luminal-type are typically 75 mg/m^2, recommended clinical doses for the HER2-positive type are 75-100 mg/m^2 and high-dose 100 mg/m^2 is used for TNBC (27,28). In the present study, the cells were treated with 053 (0, 5 or 10 μM), DOC (10 μM), DDP (50 μM), GEM (80 μM), PTX (0.1 μM) and 5-FU (50 μM) alone or combined with 053 (5 μM) for 24 h. Subsequently, the cells were collected and washed with Annexin V-FITC binding buffer (cat. no. C1062S; Beyotime Biotechnology) twice, resuspended with staining solution containing 5 μl Annexin V-FITC and 5 μl PI (cat. no. C1062S; Beyotime Biotechnology) and incubated for 30 min in the dark. Finally, cell apoptosis was assessed using flow cytometry (MoFlo XDP). FlowJo software was used for analysis.

Reactive oxygen species (ROS) assay. MCF-7 or MDA-MB-231 cells (~1x10^5/well) were seeded into 12-well plates and incubated overnight at 37˚C in a humidified

atmosphere with 5% CO_2. After which, the cells were treated with different concentrations of 053 (0, 2.5, 5 or 10 μM) for 24 h. A ROS Assay Kit (cat. no. CM-H2DCFDA; Beyotime Biotechnology) was used to detect intracellular ROS level of cells, and fluorescence was measured using a flow cytometer (MoFlo XDP). FlowJo software was used for analysis.

Multi-color flow cytometry assay. MDA-MB-231 or 4T1 cells (~1x10^5/well) were seeded into 12-well plates and incubated overnight at 37˚C in a humidified atmosphere with 5% CO_2. After which, the cells were treated with different concentrations of 053 (0, 5 and 10 μM) for 24 h. Next, MDA-MB-231 or 4T1 cells were collected for PD-L1/B7-H1-PE (cat. no. 10084-R312-P; 1:25; Beijing Sino Technology Co. Ltd) antibody labelling. T cells (~1x10^5/well) were seeded into 6-well plates and treated with concentrations of 053 (0, 5 and 10 μM) for 24 h. T cells were co-cultured with MDA-MB-231 cells at a 1:1 ratio, both of which were treated with 053 (0, 5 or 10 μM) for 24 h. Treated T cells were collected for CD3-BV650 (cat. no. A07749; 1:25; Beckman Coulter, Inc.), CD4-APC-H7 (cat. no. 737660; 1:25; Beckman Coulter, Inc.), CD8-PE-CY7 (cat. no. 6604728; 1:25; Beckman Coulter, Inc.), IFN-γ-FITC (cat. no. 11-7319-82; 1:25; eBioscience; Thermo Fisher Scientific, Inc.), Granzyme B-FITC (cat. no. 560211; 1:25; BD Pharmingen; BD Biosciences), PD-1-BV421 (cat. no. 564323; 1:25; BD Biosciences), TIM3-RB705 (cat. no. 570584; 1:25; BD Biosciences), OX-40-RB705 (cat. no. 757846; 1:25; BD Biosciences), 4-1BB-RY603 (cat. no. 759418; 1:25; BD Biosciences) and inducible T-cell Co-stimulator (ICOS-R718; cat. no. 751854; 1:25; BD Biosciences) antibody labeling. Finally, after incubating for 30 min at room temperature in the dark, the assay was performed using flow cytometry (MoFlo XDP). FlowJo software was used for analysis. The flow cytometry gating strategy involved labelling T cells with CD3 to assess the expression of PD-1, TIM3, OX-40, 4-1BB and ICOS on the surface of T cells. $CD3^+$ T cells were then separated into $CD3^+CD8^+$ T cells or $CD3^+CD4^+$ T cells, then IFN-γ and granzyme B were detected.

In vivo xenograft experiment. A total of 24 BALB/cJ female nude mice (age, 5-6 weeks; weight, 16-20 g) and 24 BALB/c female mice (age, 5-6 weeks; weight, 10-14 g) were purchased from GemPharmatech Co. Ltd. and housed in a specialized pathogen-free environment (20-25˚C; humidity, 40-60%; 12-h light/dark cycle and *ad libitum* access to food and water). Animals were checked daily and any animal found unexpectedly to be moribund, cachectic or unable to obtain food or water was sacrificed. However, no such cases occurred during the present study. The *in vivo* mouse study procedure was performed according to The Laboratory Animal Ethics Committee of The College of Biological Sciences and Engineering, Fuzhou University (Fuzhou, China; approval no. 2022-SG-022). In strict compliance with animal welfare guidelines, the tumor burden was maintained within ethical limits: Tumor weight did not exceed 10% of the mouse body weight (10% indicates: subcutaneous tumors on the backs of 25 g mice reached a diameter of ~17 mm), the average tumor diameter remained under 20 mm and the tumor volume was kept below 2,000 mm^3. After 7 days, when the mice had acclimatized to the new environment, 5x10^6 MDA-MB-231 cells were injected subcutaneously into the left hindlimbs of BALB/cJ nude mice and 2x10^6 4T1 cells were injected subcutaneously into the left hindlimbs of BALB/c mice. When the tumor volume measured ~100 mm^3 (7 days, recorded as day 0), mice were randomly divided into the following four groups (n=5/group): i) PBS (control); ii) 053; iii) GEM; and iv) 053+ GEM. During the experiment, the health and behavior of the mice were monitored daily. Following tumor formation, intravenous injections via the tail vein were administered every 3 days at a dosage of 150 μl per mouse for a period of 3 weeks, totaling 7 injections. The administered agents consisted of normal saline, 053 (10 mg/kg), GEM (10 mg/kg) or a combination of 053 (5 mg/kg) and GEM (5 mg/kg). The body weight, tumor length and width were measured every 3 days, and the tumor volume was calculated according to the formula: Tumor volume=(longest diameter x shortest diameter^2)/2. At the end of the study (21 days post-injection), mice were euthanized following deep anesthesia using isoflurane (5% for induction, 2% for maintenance). CO_2 inhalation was used to complete euthanasia at a displacement rate of 30-70% of the chamber volume per min. Following euthanasia by carbon dioxide inhalation, cervical dislocation was performed to confirm death (evidenced by a visible gap between the skull and the spine), and death was further verified by the absence of respiration. After euthanasia, the tumors, heart, liver, spleen, lungs and kidneys were excised and immediately placed in either 4% paraformaldehyde or tissue preservation solution (cat. no. HY-K6010; MedChemExpress), followed by storage at 4˚C for subsequent analysis. All mice were euthanized at the planned end of the experiment.

Tumor tissue was transferred to an Eppendorf tube and cut into small fragments. Tumor tissue digestion solution (cat. no. abs50090-10T; Absin Bioscience Inc.) was then added for digestion into a single-cell suspension. After which, the single-cell suspension was slowly added to a centrifuge tube containing 4 ml Ficoll Paque PREMIUM and centrifuged at 2,000 x g with an acceleration of 8 and a deceleration of 0 for 20 min at room temperature. The middle white membrane layer was collected and washed twice with PBS, followed by labeling with Fixable Viability Stain 510 (FVS510; cat. no. 564406; 1:1,000), CD45-APC-CY7 (cat. no. 557659; 1:25), CD3-APC (cat. no. 565643; 1:25), CD4-BV605 (cat. no. 563151; 1:25), CD8a-PE-CY7 (cat. no. 552877; 1:25), PD-1-BV421 (cat. no. 748268; 1:25), TIM3-BV650 (cat. no. 747623; 1:25), OX-40-BV605 (cat. no. 740545; 1:25), ICOS-BB515 (cat. no. 565880; 1:25) and 4-1BB-BV421 (cat. no. 740033; 1:25) (all from BD Biosciences). The tumor cells at the bottom were collected and washed twice with PBS, followed by labeling with FVS510 and PD-L1 (cat. no. 758168; 1:25; BD Biosciences). The assay was performed using flow cytometry (MoFlo XDP). FlowJo software was used for analysis. The flow cytometry gating strategy used FVS510 to identify the viable tumor cell population and detect PD-L1 expression. Viable lymphocyte populations were identified using FVS510 and CD45, followed by CD3 marking of T cells to detect the expression of PD-1, TIM3, OX-40, 4-1BB and ICOS on the surface of T cells and further detection of the proportions of $CD3^+CD8^+$ T cells and $CD3^+CD4^+$ T cells.

Biological tissue sections test. Tissues including major organs and tumors were collected from mouse xenograft models and fixed in 4% paraformaldehyde at 4˚C for 24 h, followed by paraffin embedding. Sections (5 μm) were prepared from the paraffin-embedded blocks, dewaxed in xylene and immersed in EDTA antigen retrieval buffer. Subsequently, hematoxylin and eosin (H&E) staining was performed. The sections were stained with 1% hematoxylin for 5 min at room temperature, treated with 1% acid alcohol for 45 sec and then counterstained with eosin for 2 min at room temperature. After dehydration through a graded series of ethanol (70, 85, 95 and 100%), the sections were cleared in xylene and finally mounted with neutral resin. The results were observed under an optical microscope.

For immunohistochemical detection, paraffin-embedded sections were dewaxed in xylene and rehydrated through a graded ethanol series. For antigen retrieval, the sections were heated in citrate buffer at 100˚C for 10 min. For the detection of intracellular epitopes (Ki67/LC3/p62), permeabilization was first performed with 0.1% Triton X-100 (20 min, room temperature), followed by quenching of endogenous peroxidase activity with 3% H_2O_2 (20 min, room temperature). The sections were then blocked with 5% BSA for 1 h at room temperature and subsequently incubated overnight at 4˚C with the following primary antibodies: Anti-Ki67 antibody (cat. no. GB111499-100; 1:1,000; Wuhan Servicebio Technology Co., Ltd), anti-LC3 antibody (cat. no. 81004-1-RR; 1:1,000; Proteintech Group, Inc), anti-p62 antibody (cat. no. GB11239-1-100; 1:1,000; Wuhan Servicebio Technology Co., Ltd), anti-PD-L1 antibody (cat. no. GB150059-100; 1:1,000; Wuhan Servicebio Technology Co., Ltd), anti-PD-L2 antibody (cat. no. 27406-1-AP; 1:4,000; Proteintech Group, Inc), anti-CD3 antibody (cat. no. GB11014-100; 1:1,000; Wuhan Servicebio Technology Co., Ltd), anti-CD4 antibody (cat. no. GB11064-100; 1:1,000; Wuhan Servicebio Technology Co., Ltd), anti-CD8 antibody (cat. no. GB11068; 1:1,000; Wuhan Servicebio Technology Co., Ltd), anti-4-1BB/CD137 antibody (cat. no. A2025; 1:200; ABclonal Biotech Co., Ltd), anti-CD134/OX40 antibody (cat. no. 32621-1-AP; 1:500; Proteintech Group, Inc), anti-PD1 antibody (cat. no. GB153744-100; 1:400; Wuhan Servicebio Technology Co., Ltd) and anti-TIM3 antibody (cat. no. 11872-1-AP; 1:1,000; Proteintech Group, Inc). Subsequently, the samples were incubated with HRP-conjugated goat anti-rabbit IgG (cat. no. GB23303; 1:5,000; Wuhan Servicebio Technology Co., Ltd) or HRP-conjugated goat anti-mouse IgG (cat. no. GB23301; 1:5,000; Wuhan Servicebio Technology Co., Ltd) at 37˚C for 1 h. Following this, staining was performed with DAB chromogen for 15 min (cat. no. G1211; Wuhan Servicebio Technology Co., Ltd), and hematoxylin was used as a counterstain for 3 min at room temperature. Finally, dehydration was conducted using a graded ethanol series, followed by immersion in xylene, and mounting with neutral balsam. The results were observed under an optical microscope.

Following permeabilization with Proteinase K (20 μg/ml; 37˚C, 20 min), TUNEL assay was performed using the commercial kit (cat. no. G1501; Wuhan Servicebio Technology Co., Ltd) according to the manufacturer's instructions. The sections were then directly mounted with an antifade mounting medium containing DAPI (cat. no. P0126; Beyotime Biotechnology). All section images were acquired using a fluorescence microscope.

Statistical analysis. GraphPad Prism 9.0 software (Dotmatics) or FlowJo software (v10.8.1; BD Biosciences) were used for data analysis. All results are expressed as the mean ± standard error. Statistical significance was evaluated using one-way analysis of variance and post hoc comparisons were performed using Dunnett's multiple comparisons test to compare all experimental groups against a single control group, while controlling the family-wise error rate under multiple testing conditions. $P<0.05$ was considered to indicate a statistically significant difference.

Results

Preliminary characterization of compound 053 on autophagy regulatory function. The structural formula of compound 053 is shown in Fig. 1A. The preliminary investigation was conducted using the tandem mRFP-GFP-LC3B reporter system. During autophagosome-lysosome fusion, only red fluorescence was detectable as the acidic lysosomal environment quenches GFP fluorescence while mRFP remains stable. When autophagy was inhibited, cytoplasmic yellow fluorescence of mRFP-GFP-LC3B was observed, resulting from co-localization of mRFP and GFP signals due to impaired autophagosome-lysosome fusion. In 053-treated MCF-7 cells, the number of GFP/mRFP-labeled LC3B puncta was significantly increased compared with control, with both the 053- and CQ-treated groups exhibiting enhanced yellow fluorescence, suggesting that compound 053 may regulate the autophagic process in breast cancer cells (Fig. S1C and D). The synthesis, detailed synthetic procedure and characterization of compound 053 are described in Data S1 (Figs. S2-S14).

Similar to CQ, compound 053 inhibits late autophagy in breast cancer cells. In the present study, the effects of compound 053 on the MDA-MB-231 and MCF-7 breast cancer cell lines were examined to facilitate a comparative analysis of their regulatory impacts. In the cell morphology analysis, it was found that with increased 053 concentration, cytoplasmic vacuolization was induced in MDA-MB-231 cells with the appearance of a large number of vesicles, which was accompanied by a reduction of the cell volume (Fig. 1B), suggesting that 053 may regulate autophagic flux while promoting apoptosis. To further demonstrate that 053 regulates autophagy, ultrastructural studies were performed. Compared with the control group, the number of vacuoles was increased in 053-treated MDA-MB-231 cells, and autophagic vesicles formed in the cytoplasm contained recognizable double-membrane structures and undegraded cargo (Fig. 1C).

LC3B-I/II is a protein marker that is intricately related to the autophagy process and has been used to monitor autophagy (29). The adaptor protein p62 connects autophagosomes to their substrates and serves as a molecular regulator in the process of cellular autophagy. Elevated levels of p62 typically reflect the blockage of autophagic flux (30). In addition, the accumulation of autophagosomes may be associated with the activation of autophagy or the suppression of late-stage autophagy. Therefore, the protein levels of p62 were detected

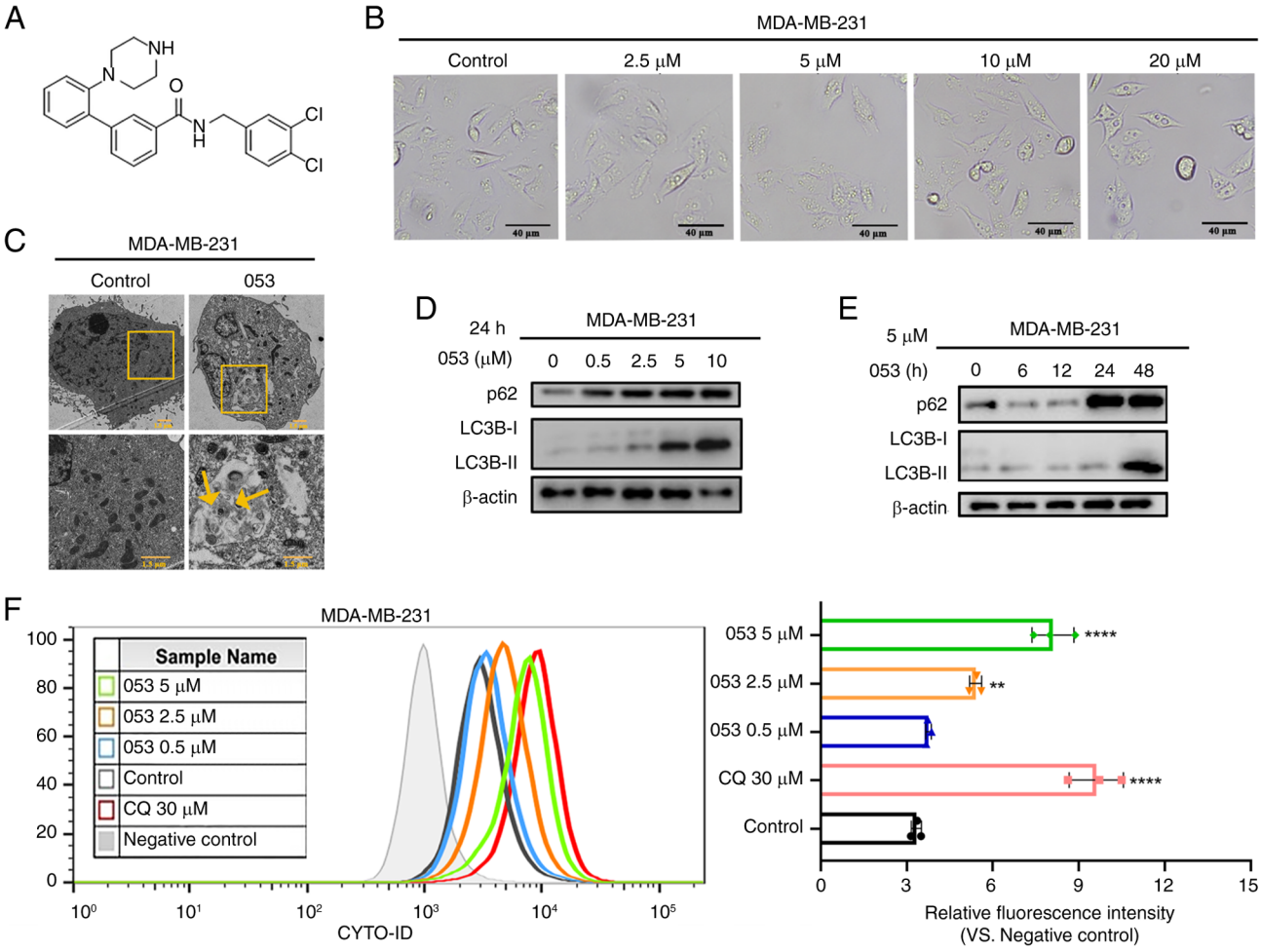

Figure 1. Compound 053 inhibits late autophagy in MDA-MB-231 cells. (A) Chemical structural formula of 053. The relative molecular mass of 053 is 440.37 g/mol. (B) Representative microscope images of MDA-MB-231 cells treated with different concentrations of 053 (0-20 μM) for 24 h. Scale bar, 40 μm. (C) Internal structure of MDA-MB-231 cells under transmission electron microscopy after treatment with 5 μM 053 for 24 h. The lower image is a magnified view of the yellow box in the image above. Scale bar, 1.5 μm. (D) Protein levels of p62 and LC3B-I/II in MDA-MB-231 cells were analyzed by western blotting after treatment with 053 (0-10 μM) for 24 h. (E) MDA-MB-231 cells were treated with 5 μM 053 for different times (0, 6, 12, 24 and 48 h), and the protein levels of p62 and LC3B-I/II were analyzed by western blotting. (F) Flow cytometry was used to detect the fluorescence intensity of autophagy-related vesicles stained with CYTO-ID in MDA-MB-231 cells. Cells were treated with 053 (0-5 μM) or CQ (30 μM) for 24 h. The bar graph shows quantitative analysis of relative fluorescence intensity. Data are presented as mean ± SEM (n=3). Statistical significance was determined by one-way ANOVA followed by Dunnett's multiple comparisons test to compare all experimental groups against a single control group. **P<0.01 and ****P<0.0001 vs. Control. 053, FZU-0045-053; p62/SQSTM1, sequestosome 1; LC3B, microtubule-associated protein 1A/1B-light chain 3B; CQ, chloroquine.

using western blotting to clarify the role of 053 in the regulation of autophagy. The results showed that the protein levels of p62 and LC3B-II exhibited an increase in a manner that was both time- and concentration-dependent following the application of 053 to MDA-MB-231 cells (Fig. 1D and E).

The CYTO-ID probe labels vacuoles associated with the autophagy pathway, whereby the green dye typically accumulates in spherical vacuoles around the nucleus. CQ, a late-stage autophagy inhibitor, primarily inhibits autophagy by blocking the fusion of autophagosomes with lysosomes (31). To further explore the role of 053 in the regulation of autophagy in both cell lines, CYTO-ID staining was conducted, followed by quantitative analysis using flow cytometry. The fluorescence intensity of CYTO-ID in MDA-MB-231 cells was gradually enhanced with increasing 053 concentration (Fig. 1F). Treatment of MCF-7 cells with 053 significantly increased vesicle accumulation, while p62 and LC3B-II protein levels exhibited time- and concentration-dependent elevation (Fig. S15A-D). Concurrently, CYTO-ID fluorescence intensity progressively increased with increasing 053 concentrations (Fig. S15E). These results demonstrated that compound 053 shares similar effects with CQ in promoting the accumulation of acidic autophagic vesicles and upregulating autophagy-related proteins (particularly p62 and LC3B-II) in breast cancer cells. These findings indicate that 053 likely suppresses late-stage autophagy by blocking autophagic flux, rather than inducing autophagy.

To confirm the effect of 053 on autophagic flux, the tandem mRFP-GFP-LC3B reporter gene was used for observation. The results demonstrated that both red and green fluorescence were enhanced by the action of 053 and CQ compared with the control group, and the yellow fluorescence was further enhanced by the co-localized superposition of red and green fluorescence. By contrast, the GFP fluorescence signal was weakened by the use of the autophagy inducer RAPA alone, and only red fluorescence could be detected by the superposition of red and green fluorescence, which indicated

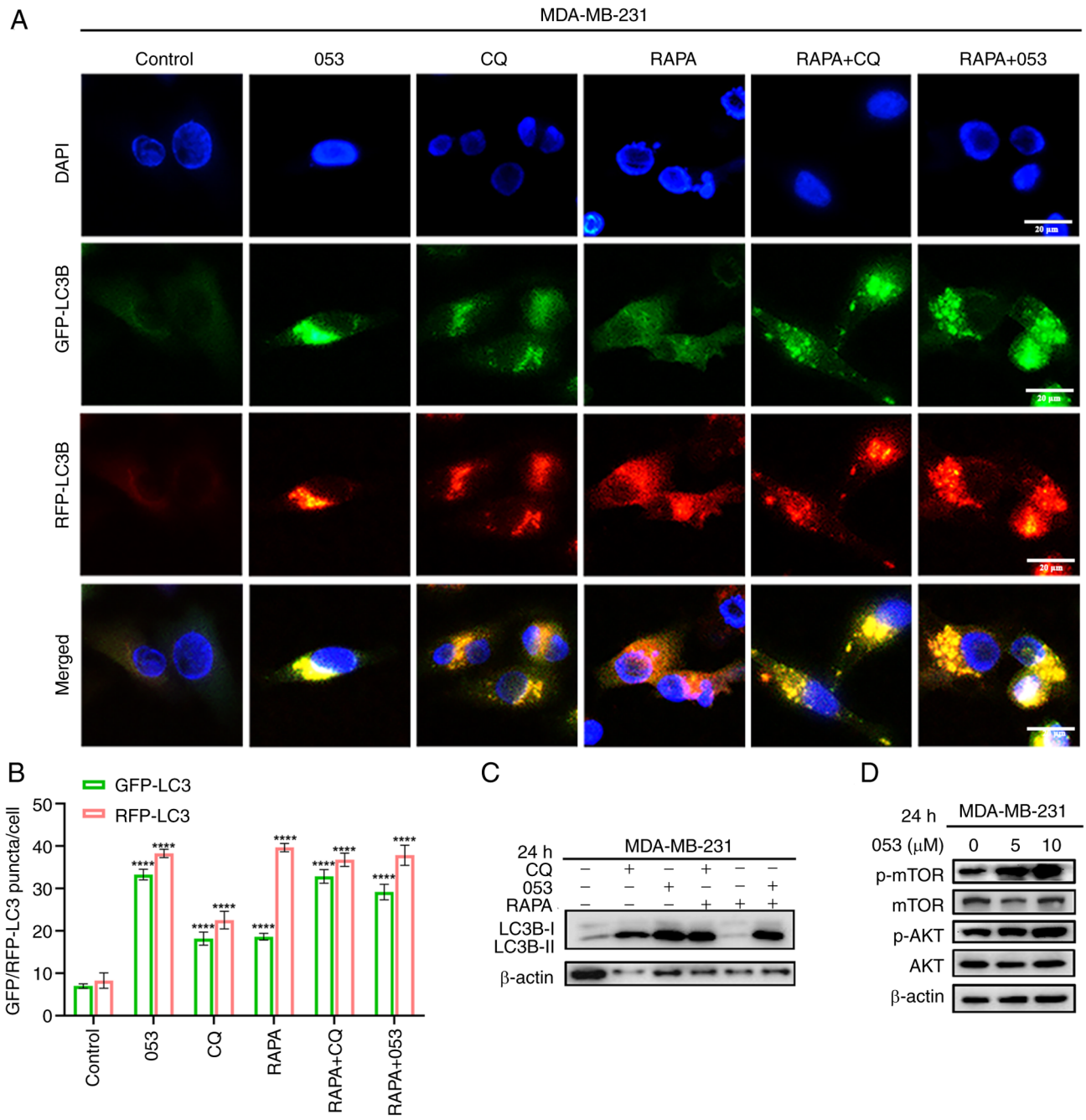

Figure 2. Compound 053 targets autophagic flux. (A) MDA-MB-231 cells were treated with RAPA (10 μM) combined with 053 (5 μM) or CQ (30 μM) or with each drug alone for 24 h. Nuclei were stained with DAPI (blue), and intracellular RFP-LC3 red fluorescence and GFP-LC3 green fluorescence were observed by inverted fluorescence microscope. Scale bar, 20 μm. (B) The number of fluorescence points was analyzed using ImageJ (1.8.0.1) software. Data are presented as mean ± SEM (n=5). Statistical significance was determined by one-way ANOVA followed by Dunnett's multiple comparisons test to compare all experimental groups against a single control group. ****P<0.0001 vs. Control. (C) MDA-MB-231 cells were treated with RAPA (10 μM) combined with 053 (5 μM) or CQ (30 μM) or with each drug alone for 24 h. The protein levels of LC3B-I/II were analyzed by western blotting. (D) MDA-MB-231 cells were treated with 053 (0-10 μM) for 24 h, the protein levels of AKT, p-AKT, mTOR and p-mTOR were analyzed by western blotting. 053, FZU-0045-053; LC3B, microtubule-associated protein 1A/1B-light chain 3B; CQ, chloroquine; RAPA, rapamycin.

that RAPA-induced autophagy accelerated autophagic flux (Figs. 2A, B, S16A and S16B). Thus, it is evident that 053, similarly to CQ, may disrupt the autophagic flux by blocking the fusion of autophagosomes and lysosomes at a late stage, leading to the accumulation of autophagosomes rather than inducing autophagy.

To further confirm that 053 is a late-stage autophagy inhibitor that functions similarly to CQ, western blotting was used to analyze the protein levels of LC3B in both cell lines following treatment with 053, CQ and RAPA. It was found that treatment with 053 or CQ alone increased the protein level of LC3B-II in cells, while the autophagy inducer RAPA did not increase the protein level of LC3B-II. This indicated that the efficiency of autophagic lysosomal degradation was not affected by RAPA treatment at this time, and that LC3B-II levels did not increase even when autophagy was activated. However, when 053 or CQ was combined with RAPA, LC3B-II protein resumed accumulation (Figs. 2C and

S16C). The PI3K/AKT/mTOR signaling pathway has been demonstrated to be a key pathway in the cellular regulation of autophagy (32). It was further verified whether the inhibitory effect of 053 on autophagy in MDA-MB-231 and MCF-7 cells was associated with the PI3K/AKT/mTOR signaling pathway. Notably, 053 specifically promoted the phosphorylation of AKT and mTOR in MDA-MB-231 cells, while not influencing the PI3K/AKT/mTOR signaling pathway in MCF-7 cells (Figs. 2D and S16D). In conclusion, these results suggested that 053 is a late autophagy inhibitor similar to CQ, which may inhibit autophagy by blocking the fusion of autophagosomes and lysosomes. The inhibitory effect of 053 on autophagy in MDA-MB-231 cells is associated with the PI3K/AKT/mTOR signaling pathway.

Compound 053 enhances chemosensitivity and downregulates PD-L1 expression in breast cancer cells. Initially, the effect of compound 053 on the viability of MCF-7 and MDA-MB-231 cells was evaluated using the CellTiter 96® AQueous One Solution assay. As shown in Figs. 3A and S17A, the results revealed that compound 053 significantly decreased the viability of 4T1, MDA-MB-231 and MCF7 cells in a dose- dependent manner. Furthermore, the effect of compound 053 on apoptosis in breast cancer cells was assessed using the Annexin-V/PI assay and it was discovered that 053 could also induce apoptosis in a concentration-dependent manner (Figs. 3B and S17B). To further investigate whether the apoptosis and autophagy inhibition induced by 053 was associated with intracellular ROS production, the effect of 053 on ROS levels in MCF-7 and MDA-MB-231 cells was assessed using a DCFH-DA probe. As shown in Figs. 3C and S17C, compound 053 did not alter ROS levels in MCF-7 and MDA-MB-231 cells, suggesting that the apoptosis and autophagy inhibition mediated by 053 is not associated with ROS levels in breast cancer cells. These findings suggest that as the concentration of 053 increased, it inhibited the proliferation of MCF-7 and MDA-MB-231 cells, while also inducing apoptosis.

Autophagy inhibition has been shown to enhance chemotherapy-induced apoptosis and suppress tumor cell proliferation, while also serving as a key mechanism of chemoresistance (11). Previously, it was demonstrated that compound 053 can inhibit late-stage autophagy. Therefore, its effect on the chemosensitivity of MDA-MB-231 cells was further investigated. Initially, the impact of compound 053 in combination with conventional breast cancer chemotherapeutic agents, including PTX, DDP, DOC, GEM and 5-FU, was assessed. Cell viability assay revealed that the combination of 053 and chemotherapeutic agents more effectively reduced the survival rate of MDA-MB-231 cells compared with treatment with either 053 or the chemotherapeutic agents alone (Fig. 3D). The Annexin V/PI assay revealed that 053 combined with chemotherapeutic drugs significantly enhanced apoptosis in MDA-MB-231 cells compared with chemotherapy alone (Fig. 3E). In conclusion, compound 053 significantly enhanced the chemosensitivity of MDA-MB-231 cells by inhibiting autophagy.

It has been reported that PD-1 and its ligand PD-L1 can be regulated by autophagy in various types of cancer (33). Tumor cells evade immune surveillance by upregulating the expression of PD-L1. PD-L1 expression in 053-treated MDA-MB-231 and 4T1 cells was examined using flow cytometry and western blotting. As shown in Fig. 3F and G, 053 treatment significantly downregulated the expression of PD-L1 on the surface of MDA-MB-231 and 4T1 cells compared with the control group. In conclusion, 053 could negatively regulate the expression of PD-L1 on the surface of MDA-MB-231 and 4T1 cells.

Compound 053 enhances the in vivo antitumor effect of GEM by inhibiting autophagy in the MDA-MB-231 xenograft nude mouse model. To more accurately simulate the *in vivo* effects of compound 053, a BALB/cJ nude mouse model for MDA-MB-231 breast cancer xenografts was established. After tumor formation, mice were injected with saline, 053 (10 mg/kg), GEM (10 mg/kg) or a combination of 053 (5 mg/kg) and GEM (5 mg/kg) via tail vein injection every 3 days for 3 weeks (Fig. 4A). As shown in Fig. 4B-D, the tumor size and weight in the control group of the nude mouse xenograft model continued to increase, while tumor growth in the drug-treated groups was inhibited to varying degrees. Notably, the tumor growth in the nude mouse xenograft model treated with the combination of 053 and GEM was the slowest and thus this treatment exhibited the most significant antitumor effect. As shown in Fig. 4E and G, immunohistochemical and immunofluorescence staining of tumor tissues from the nude mouse xenograft model revealed that, compared with the saline-treated group (control), 053 treatment alone reduced Ki67 expression and increased TUNEL expression in tumors, while the combination of 053 and GEM further decreased Ki67 expression and elevated TUNEL expression. Subsequently, the antitumor effect of 053 was further confirmed by analyzing H&E-stained tumor tissues. As shown in Fig. 4H, the tumor tissues in the control group showed almost no cell necrosis or apoptosis, whereas the 053- and GEM-treated groups displayed extensive cell shrinkage and apoptotic nuclei, and the tumor tissues in the 053- and GEM-combined treatment group exhibited the most severe cell damage. More notably, immunohistochemical staining of the tumor tissues also showed that, compared with the control group, 053 alone or in combination with GEM significantly increased the expression of LC3B and p62 in the tumor tissues (Fig. 4E). As previously demonstrated, it was confirmed that 053 can negatively regulate the expression of PD-L1in MDA-MB-231 cells *in vitro*. Therefore, the expression of PD-L1 in the tumor tissues of a nude mouse xenograft model was further tested using immunohistochemical staining. Notably, treatment with 053 alone or in combination with GEM reduced the expression of PD-L1 in tumor tissues compared with the control group (Fig. 4E). All the aforementioned results indicated that 053 can effectively inhibit the autophagy of tumor cells *in vivo*, and the combination treatment with GEM significantly enhances the antitumor effect.

In addition, there was no significant decrease in body weight in the 053-treated mice compared with the other treatment groups during the treatment period (Fig. 4F). The major organs (heart, liver, spleen, lungs and kidneys) of the treated mice were further examined using H&E staining. As shown in Fig. 4H, no obvious organ damage or inflammatory lesions were observed in mice treated with 053. However,

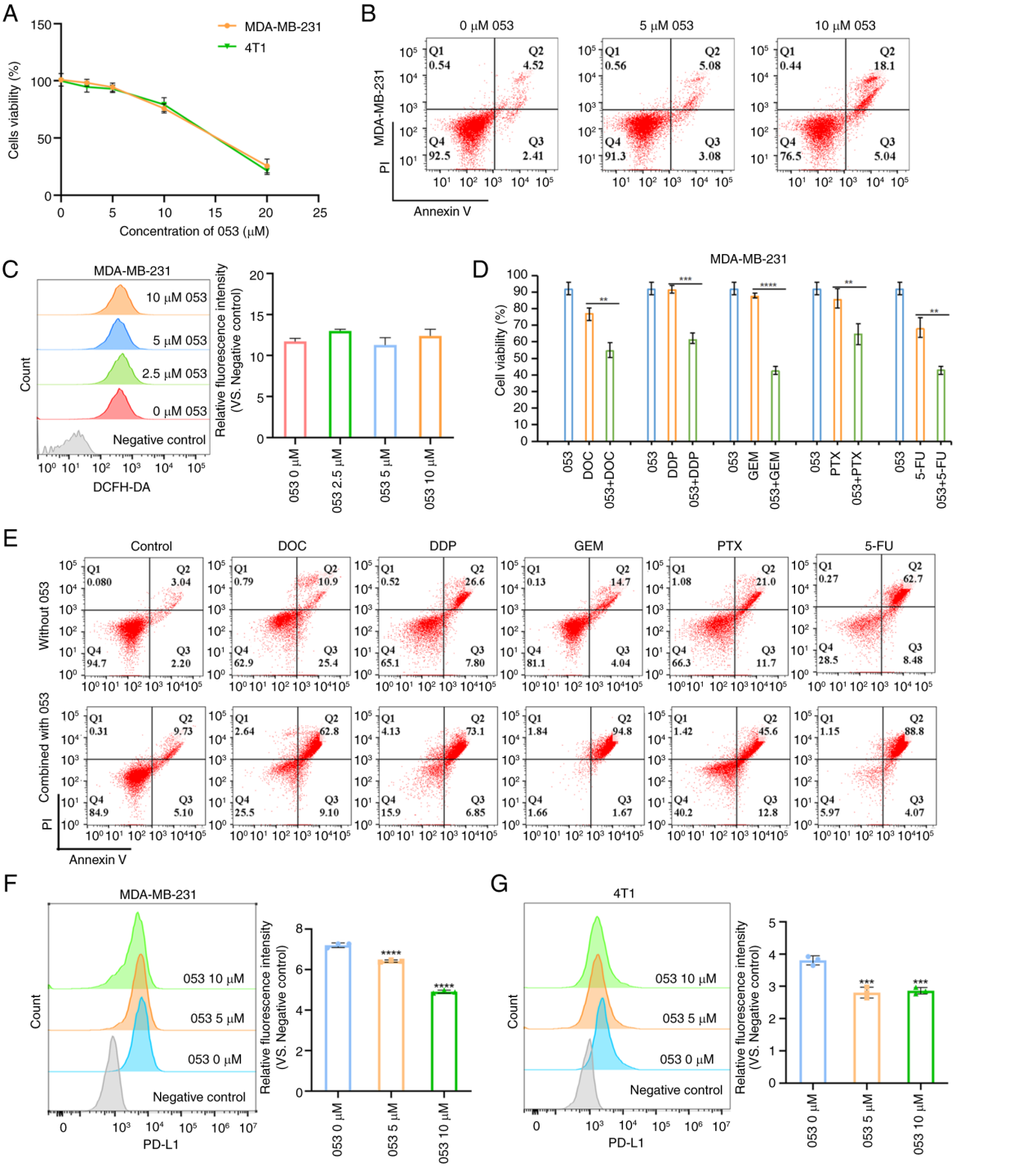

Figure 3. Compound 053 induces apoptosis and downregulates PD-L1 expression in MDA-MB-231 cells. (A) CellTiter 96® AQueous One Solution Cell Proliferation Assay was used to determine the proliferation of 4T1 and MDA-MB-231 cells treated with 053 (0-20 μM) for 24 h. (B) The apoptosis of MDA-MB-231 cells after treatment with 053 (0-10 μM) for 24 h was analyzed by flow cytometry. (C) The ROS levels in MDA-MB-231 cells after treatment with 053 (0-10 μM) for 24 h was analyzed by flow cytometry. The bar graph shows quantitative analysis of relative fluorescence intensity. Data are presented as mean ± SEM (n=3). Statistical significance was determined by one-way ANOVA followed by Dunnett's multiple comparisons test to compare all experimental groups against a single control group. (D) CellTiter 96® AQueous One Solution Cell Proliferation detection of MDA-MB-231 cell viability when treated with 053 (5 μM), DOC (10 μM), DDP (50 μM), GEM (80 μM), PTX (0.1 μM) and 5-FU (50 μM) treated alone, or the effect of 053 combined with chemotherapy drugs on the viability of MDA-MB-231 cells after 24 h treatment. Data are presented as mean ± SEM (n=4). Statistical significance was determined by one-way ANOVA followed by Dunnett's multiple comparisons test to compare all experimental groups against a single control group. **P<0.01, ***P<0.001 and ****P<0.0001. (E) Apoptosis of MDA-MB-231 cells was detected by flow cytometry, cells were treated with 053 (5 μM), DOC (10 μM), DDP (50 μM), GEM (80 μM), PTX (0.1 μM) and 5-FU (50 μM) or 053 in combination with chemotherapy drugs for 24 h. (F) Flow cytometry was used to detect PD-L1 surface expression on MDA-MB-231 cells treated with 053 (0-10 μM) for 24 h. The bar graph shows quantitative analysis of relative fluorescence intensity. Data are presented as mean ± SEM (n=3). Statistical significance was determined by one-way ANOVA followed by Dunnett's multiple comparisons test to compare all experimental groups against a single control group. ****P<0.0001 vs. 0 μM 053. (G) Flow cytometry was used to detect surface expression on 4T1 cells treated with 053 (0-10 μM) for 24 h. The bar graph shows quantitative analysis of relative fluorescence intensity. Data are presented as mean ± SEM (n=3). Statistical significance was determined by one-way ANOVA followed by Dunnett's multiple comparisons test to compare all experimental groups against a single control group. ***P<0.001 vs. 0 μM 053. 053, FZU-0045-053; ROS, reactive oxygen species; DOC, docetaxel; DDP, cisplatin; GEM, gemcitabine; PTX, paclitaxel; 5-FU, 5-fluorouracil; PD-L1, programmed death-ligand 1.

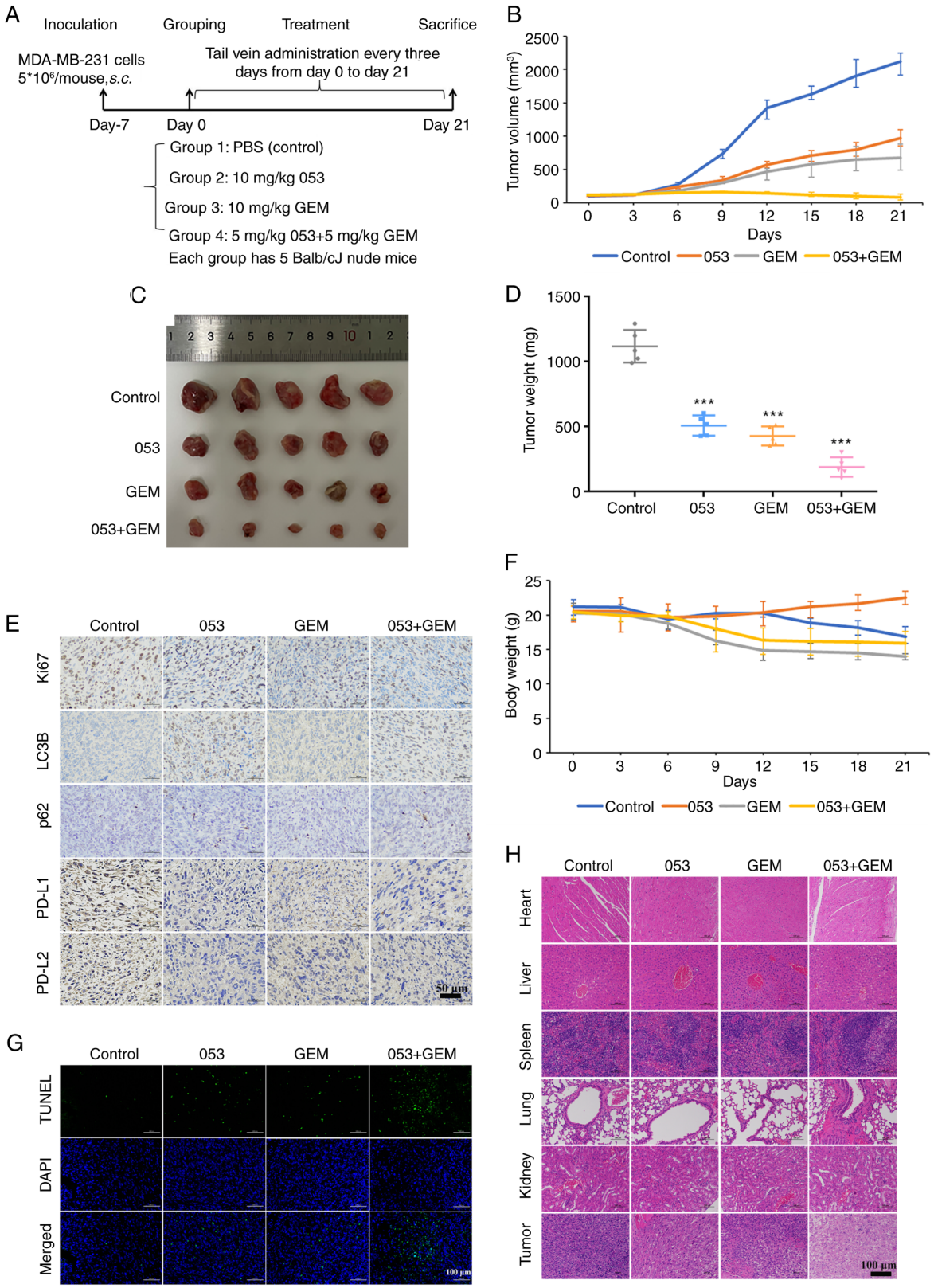

Figure 4. Compound 053 enhances the therapeutic effect of GEM by inhibiting autophagy in the MDA-MB-231 xenograft model. (A) Mouse treatment plan. (B) The tumor size was measured with a caliper every 3 days and the volume was calculated (n=5). (C) Tumor morphology of mouse removed at 21 days of treatment. (D) The tumors were removed and weighed at 21 days of treatment. Data are presented as mean ± SEM (n=5). Statistical significance was determined by one-way ANOVA followed by Dunnett's multiple comparisons test to compare all experimental groups against a single control group. ***P<0.001 vs. Control. (E) Protein levels of Ki67, LC3B, p62, PD-L1 and PD-L2 were detected using immunohistochemical staining in tumor tissues of mice after 21 days of treatment. Nuclei are localized in blue and target proteins are localized in brown. Scale bar, 50 μm. (F) Body weight was measured every 3 days. (G) The TUNEL assay was used to evaluate DNA fragmentation in mouse tumor tissues after 21 days of treatment. Blue fluorescence indicates nuclear staining (DAPI), while green fluorescence specifically labels DNA breaks associated with apoptosis. Scale bar, 100 μm. (H) H&E staining of tumor tissues and major organs (heart, liver, spleen, lungs and kidneys) of mice after 21 days of treatment. Nuclei are blue-purple and cytoplasm is red. Scale bar, 100 μm. 053, FZU-0045-053; GEM, gemcitabine; LC3B, microtubule-associated protein 1A/1B-light chain 3B; p62/SQSTM1, sequestosome 1; PD-L1/2, programmed death-ligand 1/2.

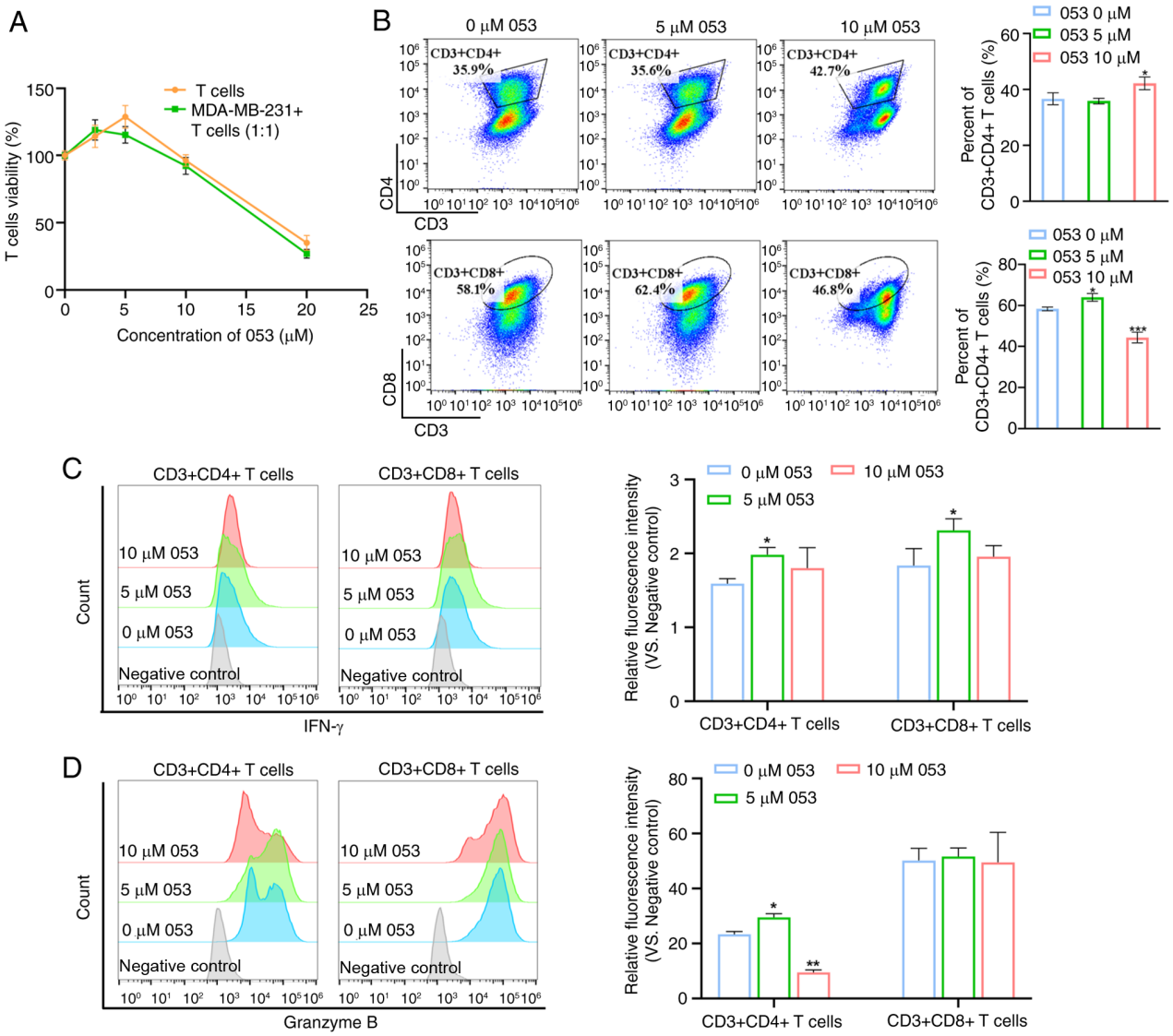

Figure 5. Compound 053 promotes T cell activation and proliferation. (A) T cells were treated with 053 (0-20 μM) for 24 h, or MDA-MB-231 cells were co-cultured with T cells followed by treatment with 053 (0-20 μM) for 24 h. T cell proliferation was assessed using an ATP detection kit. (B) Flow cytometry was used to analyze the differentiation of $CD3^+CD4^+$ T cells and $CD3^+CD8^+$ T cells after 24 h treatment with 053 (0-10 μM). The bar graph shows the percentage of $CD3^+CD4^+$ T cells and $CD3^+CD8^+$ T cells. Data are presented as mean ± SEM (n=3). Statistical significance was determined by one-way ANOVA followed by Dunnett's multiple comparisons test to compare all experimental groups against a single control group. $^*P<0.05$ and $^{***}P<0.001$ vs. 0 μM 053. (C) Flow cytometry was used to analyze IFN-γ production in T cells after 24 h treatment with 053 (0-10 μM). The bar graph shows quantitative analysis of relative fluorescence intensity. Data are presented as mean ± SEM (n=3). Statistical significance was determined by one-way ANOVA followed by Dunnett's multiple comparisons test to compare all experimental groups against a single control group. $^*P<0.05$ vs. 0 μM 053. (D) Flow cytometry was used to analyze Granzyme B production in T cells after 24 h treatment with 053 (0-10 μM). The bar graph shows quantitative analysis of relative fluorescence intensity. Data are presented as mean ± SEM (n=3). Statistical significance was determined by one-way ANOVA followed by Dunnett's multiple comparisons test to compare all experimental groups against a single control group. $^*P<0.05$ and $^{**}P<0.01$ vs. 0 μM 053. 053, FZU-0045-053.

mice treated with GEM showed mild inflammation in the liver, irregular arrangement of alveolar epithelial cells, diffuse alveolar damage and interstitial edema. These results indicate that 053 exhibits greater biosafety in mice compared with the conventional chemotherapeutic agent GEM. In summary, 053 exhibits high biosafety *in vivo* and enhances the antitumor effect by inhibiting autophagy in tumor cells while negatively regulating the expression of PD-L1 in tumor tissues.

Compound 053 promotes T cell activation and proliferation by regulating co-stimulatory and co-inhibitory molecules on the surface of T cells. The dose-response experiments demonstrated that low dose 053 (0-5 μM) promoted T cell proliferation, while higher concentrations (>5 μM) induced cytotoxicity. Notably, this biphasic effect was replicated in the T cell-tumor cell (MDA-MB-231) co-culture system, indicating that 5 μM 053 optimally activated T cell expansion in both isolated and tumor-associated environments (Fig. 5A). Therefore, it was hypothesized that compound 053 exhibits immunomodulatory potential. Subsequently, it was observed that treatment with 5 μM 053 did not alter the proportion of $CD4^+$ T cells but slightly increased the proportion of $CD8^+$ T cells. Notably, treatment with 10 μM 053 reduced the proportion of $CD8^+$ T cells, while increasing the proportion of $CD4^+$ T cells (Fig. 5B). Activated $CD4^+$ T cells and $CD8^+$ T cells secrete a range of cytokines involved in inflammatory

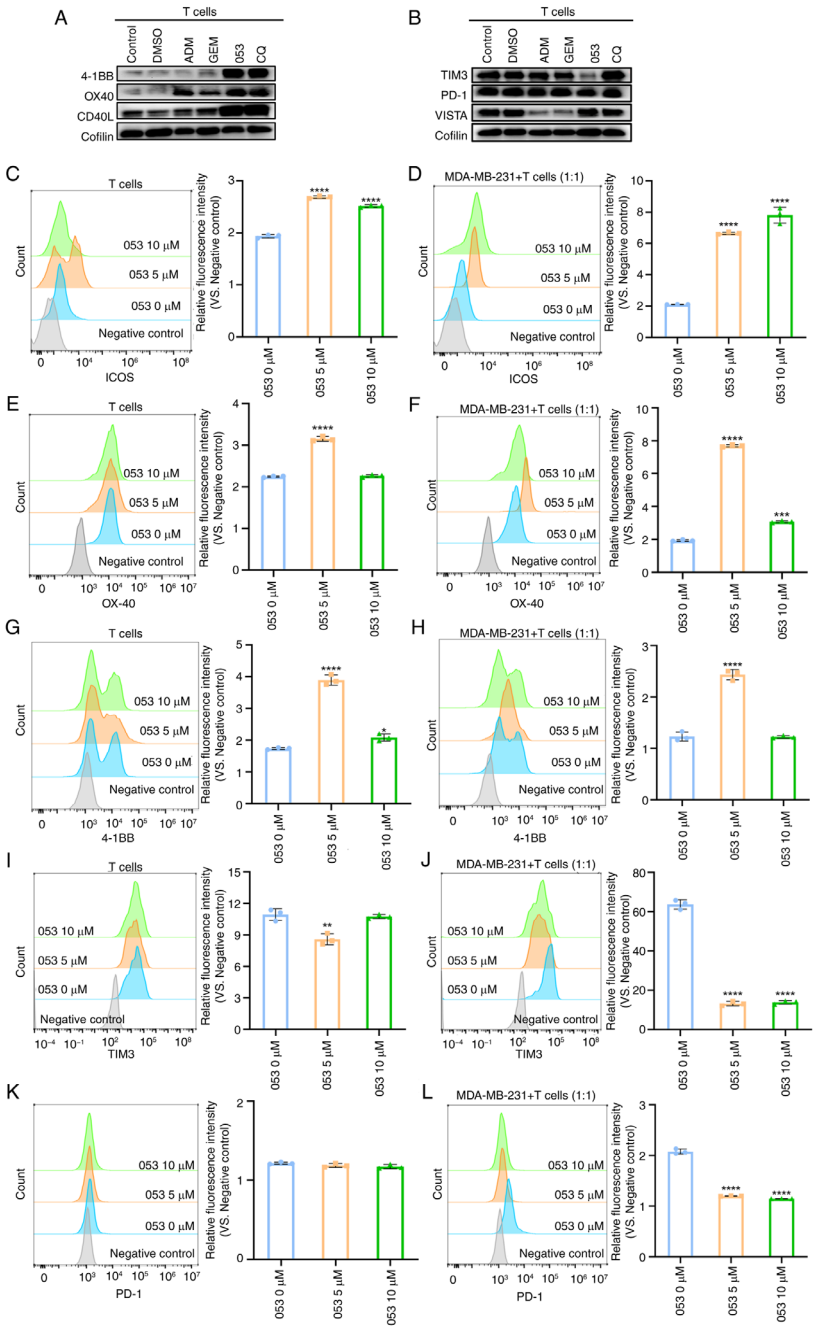

Figure 6. Compound 053 modulates co-stimulatory and co-inhibitory molecules on T cell surfaces. (A) The protein levels of 4-1BB, OX40 and CD40L after 5 μM ADM, GEM (80 μM), 053 (5 μM) or CQ (30 μM) treatment were analyzed by western blotting. (B) The protein levels of TIM3, PD-1 and VISTA after 5 μM ADM, GEM (80 μM), 053 (5 μM) or CQ (30 μM) treatment were analyzed by western blotting. (C) After T cells were treated with 053 (0-10 μM) for 24 h, ICOS expression on T cell surfaces was analyzed by flow cytometry. The bar graph shows quantitative analysis of relative fluorescence intensity. (D) T cells were co-cultured with MDA-MB-231 cells at a 1:1 ratio and treated with 053 (0-10 μM) for 24 h, followed by flow cytometric analysis of ICOS expression on T cell surfaces. The bar graph shows quantitative analysis of relative fluorescence intensity. (E) After T cells were treated with 053 (0-10 μM) for 24 h, OX-40 expression on T cell surfaces was analyzed by flow cytometry. The bar graph shows quantitative analysis of relative fluorescence intensity. (F) T cells were co-cultured with MDA-MB-231 cells at a 1:1 ratio and treated with 053 (0-10 μM) for 24 h, followed by flow cytometric analysis of OX-40 expression on T cell surfaces. The bar graph shows quantitative analysis of relative fluorescence intensity. (G) After T cells were treated with 053 (0-10 μM) for 24 h, 4-1BB expression on T cell surfaces was analyzed by flow cytometry. The bar graph shows quantitative analysis of relative fluorescence intensity. (H) T cells were co-cultured with MDA-MB-231 cells at a 1:1 ratio and treated with 053 (0-10 μM) for 24 h, followed by flow cytometric analysis of 4-1BB expression on T cell surfaces. The bar graph shows quantitative analysis of relative fluorescence intensity. (I) After T cells were treated with 053 (0-10 μM) for 24 h, TIM3 expression on T cell surfaces was analyzed by flow cytometry. The bar graph shows quantitative analysis of relative fluorescence intensity. (J) T cells were co-cultured with MDA-MB-231 cells at a 1:1 ratio and treated with 053 (0-10 μM) for 24 h, followed by flow cytometric analysis of TIM3 expression on T cell surfaces. The bar graph shows quantitative analysis of relative fluorescence intensity. (K) After T cells were treated with 053 (0-10 μM) for 24 h, PD-1 expression on T cell surfaces was analyzed by flow cytometry. The bar graph shows quantitative analysis of relative fluorescence intensity. (L) T cells were co-cultured with MDA-MB-231 cells at a 1:1 ratio and treated with 053 (0-10 μM) for 24 h, followed by flow cytometric analysis of PD-1 expression on T cell surfaces. The bar graph shows quantitative analysis of relative fluorescence intensity. Data are presented as mean ± SEM (n=3). Statistical significance was determined by one-way ANOVA followed by Dunnett's multiple comparisons test to compare all experimental groups against a single control group. *P<0.05, **P<0.01, ***P<0.001, ****P<0.0001 vs. 0 μM 053. 053, FZU-0045-053; ADM, adriamycin; 4-1BB, tumor necrosis factor receptor superfamily member 9; OX40, tumor necrosis factor receptor superfamily member 4; CD40L, CD40 ligand; ICOS, inducible T-cell co-stimulator; PD-1, programmed cell death protein 1; TIM3, T-cell immunoglobulin and mucin-domain containing-3; VISTA, V-domain Ig suppressor of T cell activation; GEM, gemcitabine; CQ, chloroquine.

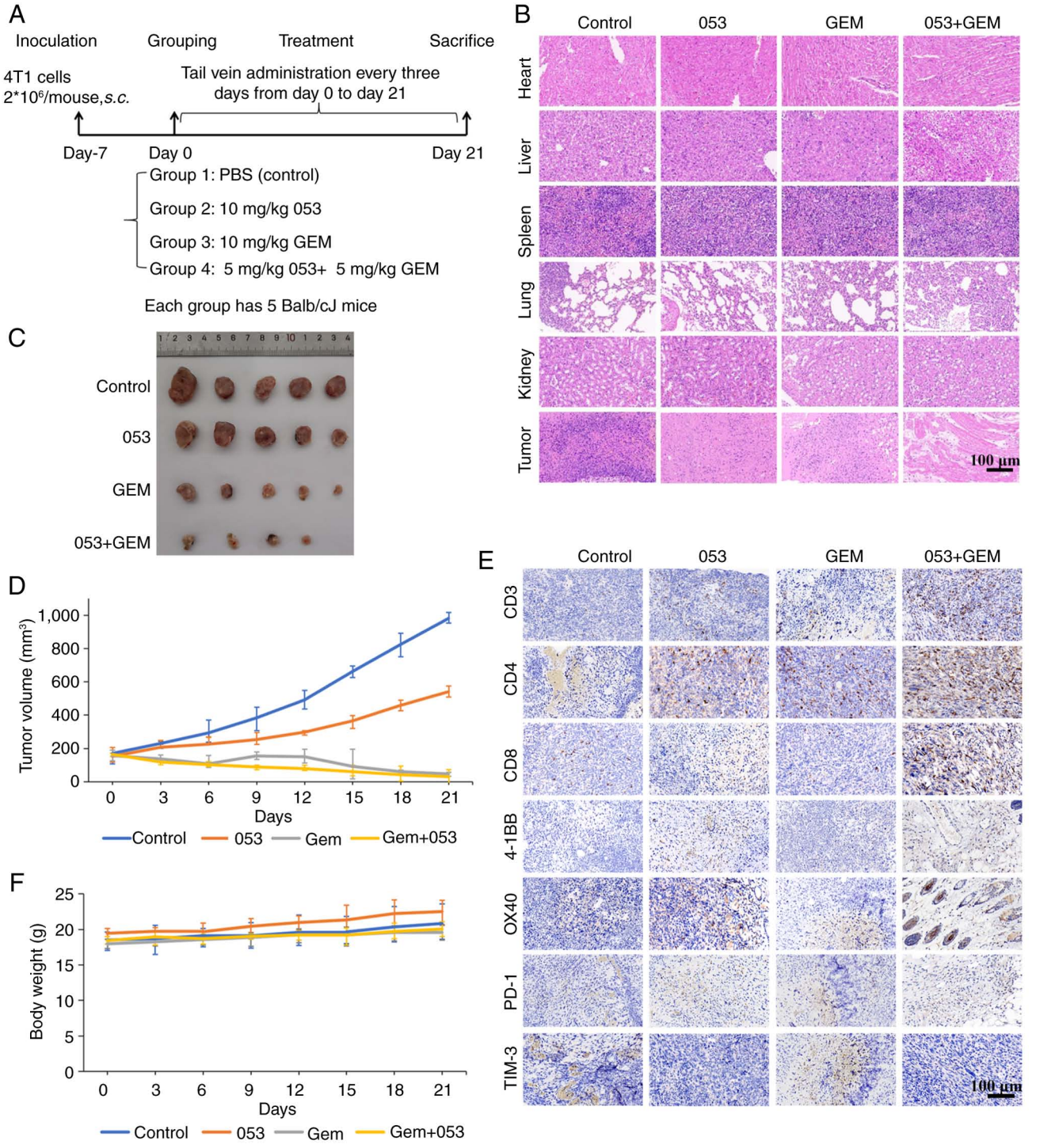

Figure 7. Compound 053 enhances the *in vivo* antitumor effect of GEM in the 4T1 xenograft model. (A) Mouse treatment plan. (B) H&E staining of heart, liver, spleen, lung and kidney. Scale bar, 100 μm. (C) Tumor morphology of mouse removed at 21 days of treatment. (D) The tumor size was measured with a caliper every 3 days and the volume was calculated (n=5). (E) Protein levels of CD3, CD4, CD8, 4-1BB, OX40, PD-1 and TIM3 were detected using immunohistochemical staining in tumor tissues of mice after 21 days of treatment. Nuclei are localized in blue and target proteins are localized in brown. Scale bar, 100 μm. (F) Body weight was measured every 3 days (n=5). 053, FZU-0045-053; GEM, gemcitabine; 4-1BB, tumor necrosis factor receptor superfamily member 9; OX40, tumor necrosis factor receptor superfamily member 4; PD-1, programmed cell death protein 1; TIM3, T-cell immunoglobulin and mucin-domain containing-3.

responses and immunomodulation. As shown in Fig. 5C and D, using flow cytometry it was found that 5 μM 053 promoted the expression of IFN-γ and Granzyme B in T cells, but 10 μM 053 downregulated the expression of IFN-γ and Granzyme B in T cells, which was due to the toxicity of high concentrations of compound 053 to T cells.

Co-stimulatory molecules on the surface of T cells, such as 4-1BB, OX-40 and CD40L, transmit positive signals by binding to their respective ligands, thereby promoting T cell activation and participation in subsequent immune responses (34). By contrast, co-inhibitory molecules on the surface of T cells, such as TIM3, PD-1 and VISTA, downregulate or terminate

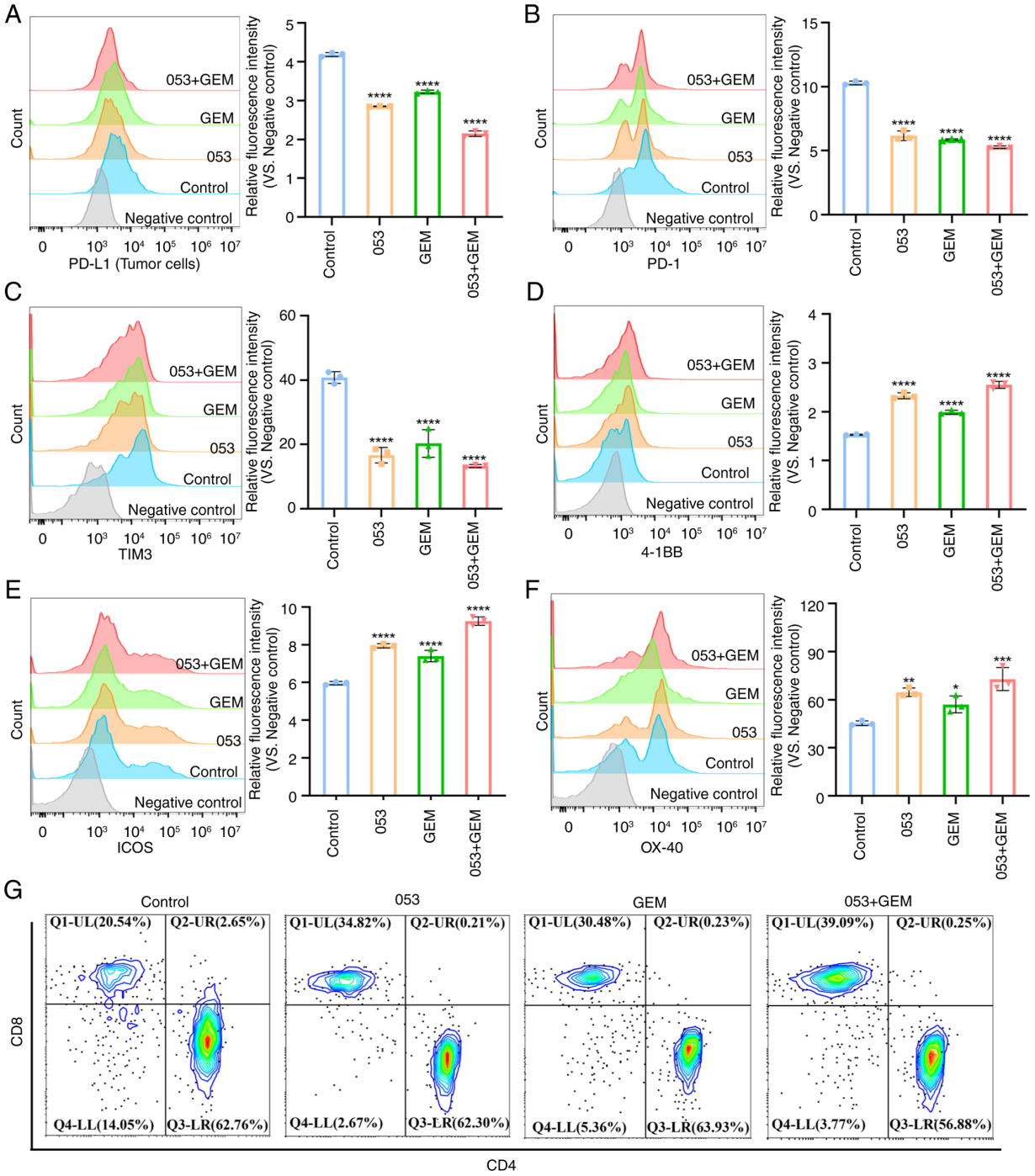

Figure 8. Compound 053 modulates PD-L1 on tumor cells and co-stimulatory/co-inhibitory molecules on tumor-infiltrating T cells in the 4T1 xenograft model. (A) Flow cytometry was performed to analyze PD-L1 surface expression on tumor cells. The bar graph shows quantitative analysis of relative fluorescence intensity. (B) PD-1 expression on tumor-infiltrating T cells surfaces was analyzed by flow cytometry. The bar graph shows quantitative analysis of relative fluorescence intensity. (C) TIM3 expression on tumor-infiltrating T cells surfaces was analyzed by flow cytometry. The bar graph shows quantitative analysis of relative fluorescence intensity. (D) 4-1BB expression on tumor-infiltrating T cells surfaces was analyzed by flow cytometry. The bar graph shows quantitative analysis of relative fluorescence intensity. (E) ICOS expression on tumor-infiltrating T cells surfaces was analyzed by flow cytometry. The bar graph shows quantitative analysis of relative fluorescence intensity. (F) OX-40 expression on tumor-infiltrating T cells surfaces was analyzed by flow cytometry. The bar graph shows quantitative analysis of relative fluorescence intensity. Data are presented as mean ± SEM (n=3). Statistical significance was determined by one-way ANOVA followed by Dunnett's multiple comparisons test to compare all experimental groups against a single control group. *P<0.05, **P<0.01, ***P<0.001, ****P<0.0001 vs. 0 μM 053. (G) Flow cytometry was used to analyze the differentiation of CD3^{+}CD4^{+} T cells and CD3^{+}CD8^{+} T cells. 053, FZU-0045-053; 4-1BB, tumor necrosis factor receptor superfamily member 9; OX40, tumor necrosis factor receptor superfamily member 4; ICOS, inducible T-cell co-stimulator; PD-1, programmed cell death protein 1; TIM3, T-cell immunoglobulin and mucin-domain containing-3; GEM, gemcitabine; PD-L1, programmed death-ligand 1.

T cell activation and proliferation by transmitting inhibitory signals (35). Western blotting was performed to evaluate the effects of compound 053, ADM, GEM and CQ on the protein levels of co-stimulatory and co-inhibitory molecules on the surface of T cells. As shown in Fig. 6A and B, it was found that compound 053 (5 μM) upregulated the expression levels of

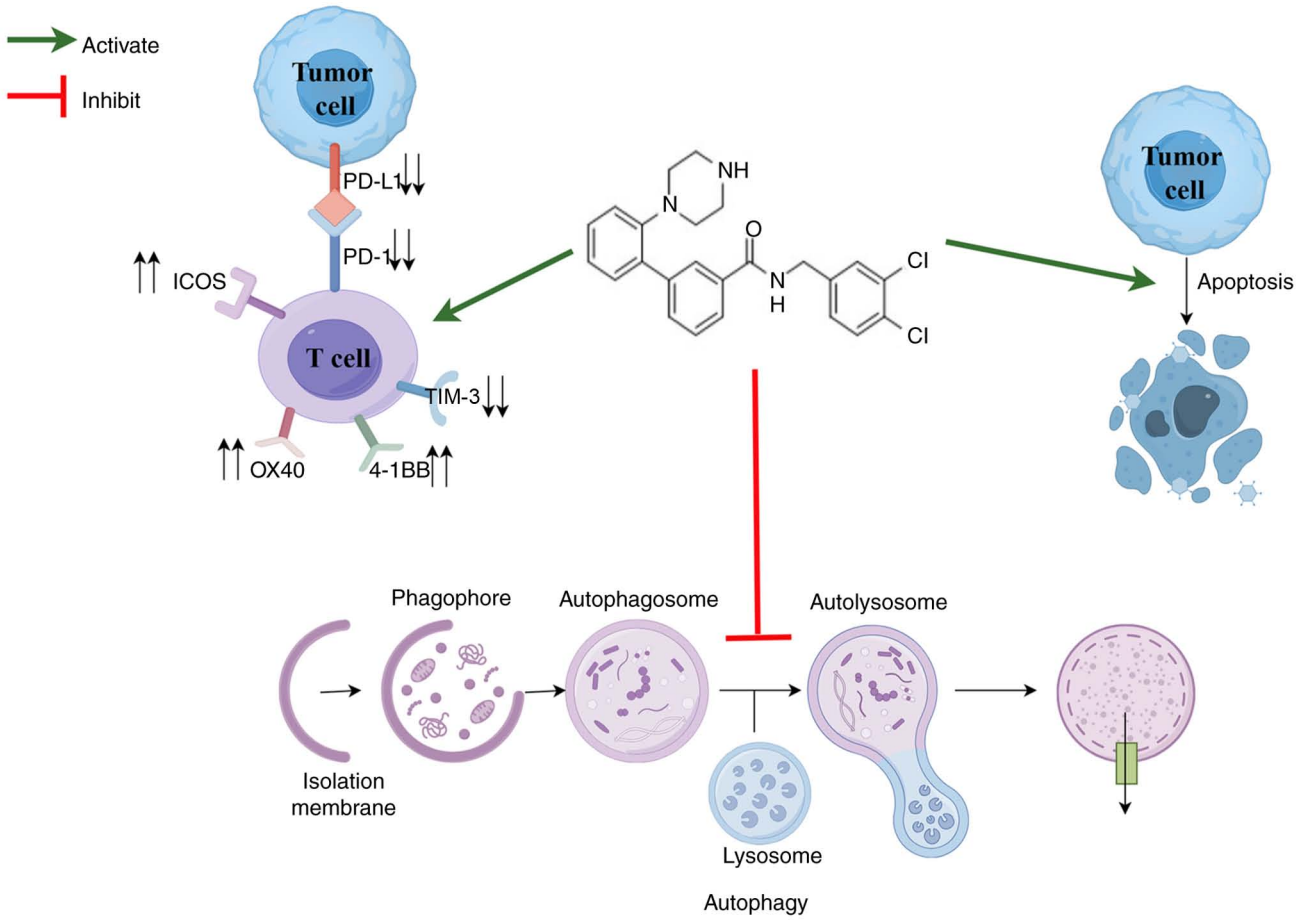

Figure 9. Mechanism of compound 053 regulating autophagy and immune response to inhibit breast cancer. 053 can inhibit autophagy and promote apoptosis of breast cancer cells. 053 also downregulated PD-L1 expression in breast cancer cells, while promoting T cell activation and proliferation by upregulating co-stimulatory molecules (4-1BB, OX40 and ICOS) and downregulating co-inhibitory molecules (TIM-3 and PD-1) on the surface of the T cells. (By Figdraw). 4-1BB, tumor necrosis factor receptor superfamily member 9; OX40, tumor necrosis factor receptor superfamily member 4; ICOS, inducible T-cell co-stimulator; PD-1, programmed cell death protein 1; TIM3, T-cell immunoglobulin and mucin-domain containing-3; PD-L1, programmed death-ligand 1.

4-1BB, CD40L and OX-40, while they decreased the levels of TIM3 on the surface of T cells. However, treatment with 053 did not alter the expression level of PD-1 and VISTA on the surface of T cells, and the levels of TIM-3, VISTA and PD-1 in the CQ group also appeared unchanged. Flow cytometry further validated that 053 (0-10 μM) treatment upregulated co-stimulatory molecules (4-1BB, ICOS and OX-40) and downregulated inhibitory markers (TIM-3) in T cells cultured alone or with MDA-MB-231 cells, with optimal effects at 5 μM (Fig. 6C-J). When T cells were treated with compound 053 in a monoculture system, the expression level of PD-1 remained unchanged. However, when 053 was applied to a co-culture system of T cells and MDA-MB-231 cells, it downregulated the surface expression of PD-1 on T cells (Fig. 6K and L). In conclusion, compound 053 regulated the activation and proliferation of T cells by downregulating the co-inhibitory molecules TIM3 and PD-1, and upregulating the co-stimulatory molecules 4-1BB, OX40, CD40L and ICOS to promote immune responses.

Compound 053 enhances the in vivo antitumor efficacy of GEM by modulating co-stimulatory and co-inhibitory molecules on tumor-infiltrating T cells in the 4T1 xenograft model. To more accurately simulate the *in vivo* antitumor effects of compound 053 through immunomodulation, a BALB/c mouse 4T1 breast cancer xenograft model was established. After tumor formation, mice were injected via the tail vein with saline, 053 (10 mg/kg), GEM (10 mg/kg) or a combination of 053 (5 mg/kg) and GEM (5 mg/kg) every 3 days for 3 weeks (Fig. 7A). As shown in Fig. 7C and D, consistent with the trends observed in the previously described nude mouse xenograft model, tumor growth was inhibited to varying degrees in the drug-treated groups compared with the control group. Notably, the combination treatment of 053 and GEM exhibited the slowest tumor growth (Fig. 7C and D). In addition, there was no significant decrease in body weight in the mice treated with 053 compared with the other treatment groups (Fig. 7F). H&E staining was used for the histological examination of major organs in mice, and no significant detrimental effects were observed at the therapeutic dose of 053 (Fig. 7B). Subsequently, analysis of the H&E staining of the tumor tissues, which was also consistent with the trend observed in the aforementioned nude mouse xenograft model, revealed that the 053 and GEM-treated groups exhibited extensive cell atrophy and nuclear apoptosis compared with the control group, with the tumor tissues of the 053 and GEM combination treatment group showing the most severe cell damage (Fig. 7B). In addition, immunohistochemical analysis of the tumors revealed that 053 increased the levels of CD3,

CD4, CD8, 4-1BB and OX-40 in the tumor tissues, while the levels of PD-1 and TIM3 were reduced, particularly when 053 was combined with GEM (Fig. 7E).

Subsequently, tumor tissues were digested into single-cell suspensions and tumor cells were separated from lymphocytes using Ficoll density gradient centrifugation. Flow cytometric analysis revealed that both the 053 monotherapy group and the 053+ GEM combination therapy group showed reduced PD-L1 expression on tumor cells (Fig. 8A). As shown in Fig. 8B-F, flow cytometric analysis further validated the aforementioned findings, demonstrating that both the 053 monotherapy group and the 053+ GEM combination therapy group exhibited increased expression of co-stimulatory molecules (4-1BB, ICOS and OX-40) on tumor-infiltrating T cells, along with decreased expression of co-inhibitory molecules (PD-1 and TIM-3). Moreover, flow cytometric analysis revealed an increase in the proportion of tumor-infiltrating $CD3^+CD8^+$ T cells in both the 053 monotherapy group and the 053+ GEM combination therapy group, rising from 20.54 to 34.82 and 39.09% (Fig. 8G). Notably, the combination therapy group showed more pronounced effects than monotherapy. In summary, these findings demonstrate that compound 053 downregulates PD-L1 expression on tumor cells while modulating co-stimulatory and co-inhibitory molecules on tumor-infiltrating T cells. This dual mechanism promotes T cell activation and proliferation, enhances effector functions and increases cytotoxic $CD8^+$ T cell infiltration in tumor tissues, ultimately potentiating its antitumor efficacy.

Discussion

To the best of our knowledge, CQ/HCQ is the only clinically approved autophagy inhibitor. However, its efficacy remains unsatisfactory in current clinical trials for various cancer types (13,36). Consequently, there is a need to develop additional autophagy modulators with novel antitumor potential. Different autophagy inhibitors target different stages of autophagy. For example, CQ and Bafilomycin A1 primarily inhibit the final stage of autophagy by blocking autophagosome-lysosome fusion, leading to the accumulation of autophagic vesicles in cells, while 3-methyladenine mainly inhibits early autophagy by preventing autophagosome formation (31,37,38). Among the more common autophagy inhibitors that block the fusion of autophagosomes and lysosomes, CQ was selected as a positive control in the present study. Research indicates that CQ increases the levels of LC3-II and p62 proteins, enhances autophagosome formation and promotes apoptosis, pretreatment with RAPA mitigates these effects (39). Notably, the present study found that both 053 and CQ treatments increased the levels of LC3B-II and p62 proteins, as well as increased the accumulation of acidic autophagosomes. Consequently, we hypothesized that 053, similar to CQ, may be a late autophagy inhibitor. Subsequently, it was investigated whether 053 affects the fusion of autophagosomes and lysosomes using a tandem mRFP-GFP-LC3B reporter gene assay. The results showed that both 053 and CQ enhanced yellow fluorescence following co-localization stacking. Consequently, it was speculated that 053, similar to CQ, disrupts autophagic flux at late stages by blocking autophagosome-lysosome fusion, which leads to the accumulation of autophagosomes. It has been reported that autophagy can be regulated through the PI3K/AKT/mTOR signaling pathway, and the inhibition of this pathway downregulates p62 expression in breast cancer cells, thereby inducing autophagy (9). Additionally, the natural product astragaloside II overcomes DDP resistance in hepatocellular carcinoma cells by inactivating autophagy through the enhancement of the PI3K/AKT/mTOR pathway (32). The results of the present study also suggest that 053 inhibits autophagy by activating the PI3K/AKT/mTOR signaling pathway in MDA-MB-231 cells. However, no significant activation of this pathway was observed in MCF-7 cells. It has been reported that autophagy regulators can modulate autophagy through both mTOR-dependent and mTOR-independent pathways (40). Therefore, we hypothesize that the autophagy-regulating effect of 053 on MCF-7 cells may not be dependent on the AKT/mTOR pathway.

Research indicates that the development of multidrug resistance frequently results from prolonged chemotherapy regimens. Additionally, the suppression of autophagy has been demonstrated to improve the effectiveness of chemotherapy, targeted therapies and immunotherapies, thereby enhancing antitumor responses (41). Consequently, after confirming that 053 is an autophagy inhibitor, the present study further investigated whether 053 enhances the sensitivity of chemotherapeutic agents by inhibiting autophagy. The results showed that 053 treatment alone induced tumor cell apoptosis in a time- and concentration-dependent manner, and the combination of 053 with chemotherapeutic agents had a significant synergistic effect, further inducing apoptosis in breast cancer cells. Furthermore, in the MDA-MB-231 xenograft nude mouse model, 053 treatment alone induced apoptosis and inhibited autophagy in tumor cells, resulting in a certain antitumor effect, and the antitumor effect was more pronounced when 053 was combined with the chemotherapeutic agent GEM. High levels of ROS have been reported to increase autophagosome formation and damage in cells (42). However, the results of the present study were inconsistent with this finding, as 053 did not affect ROS levels in tumor cells, suggesting that 053 does not depend on the ROS pathway to regulate autophagy and apoptosis in breast cancer cells.

The expression of PD-L1 is related to autophagy mediated by LC3 and p62. There is a strong negative correlation between p62 and PD-L1 (9). Notably, the present study demonstrated that compound 053 inhibited autophagy in tumor cells by increasing the protein levels of LC3-II and p62, while simultaneously downregulating PD-L1 expression. Research has shown that knocking out the autophagy-related gene Rb1cc1 in tumor cells to inhibit autophagy increases TNFα-mediated T cell killing of tumor cells and enhances the efficacy of immune checkpoint blockade in mouse tumor models (43). Immune checkpoint blockade in tumor immunotherapy has been reported to enhance antitumor T-cell responses through anti-PD-1, anti-CTLA-4 or anti-PD-L1 therapy (20). T cell co-stimulation is mediated by immunoregulatory molecules (CD28, CD40L, CD30, OX40 and 4-1BB) expressed on T lymphocytes, while co-inhibitory receptors (PD-1, CTLA-4, VISTA and TIM3) induce T cell dysfunction and abrogate antitumor immunity (9,19,34,35). The results of the *in vivo* and *in vitro* experiments in the present study showed that 053 upregulated the expression levels of 4-1BB and OX-40 while decreasing the levels of PD-1 and TIM-3 on the surface of T cells, and the effect was more pronounced when 053 was combined with GEM *in vivo*. Furthermore, autophagy

deficiency leads to the accumulation of cytoplasmic DNA (such as the release of mitochondrial DNA), blocking STING degradation and promoting the secretion of type I interferons and pro-inflammatory factors through the cGAS/STING pathway, which enhances $CD8^+$ T cell infiltration (44,45). The results of the present study further indicated that compound 053 upregulated the expression of IFN-γ and Granzyme B in T cells, thereby promoting T cell activation and proliferation. In the 4T1 xenograft model, treatment with 053 significantly enhanced the infiltration of $CD8^+$ T cells into tumor tissues. IRGQ-mediated autophagy inhibition can reduce the degradation of MHC class I molecules, enhance tumor antigen presentation and promote T cell recognition (46). This aligns with the findings of the present study in which compound 053 not only inhibited tumor cell autophagy but also exhibited immunostimulatory properties. Therefore, the regulatory effect of autophagy deficiency in tumor cells on immune responses is likely secondary. However, the mechanistic link between autophagy inhibition and immune regulation in the present study still needs further validation, such as knocking out key autophagy genes in TNBC cells to explore whether 053 has similar immune regulatory effects.

In conclusion, in the present study, small molecule compounds were selected to investigate their modulatory effects on autophagy and immune responses in tumor. Notably, the results showed that the small molecule compound 053 not only inhibited autophagy but also downregulated the expression of PD-L1 while promoting the activation and proliferation of T cells by regulating co-stimulatory and co-inhibitory molecules on the surface of T cells (Fig. 9). This compound activated antitumor immunity while inhibiting autophagy, blocking the self-protective mechanisms of tumor cells under chemotherapy stress, thereby enhancing their sensitivity to treatment. For difficult-to-treat subtypes of breast cancer, such as TNBC, this compound may fill the gap in existing immunotherapy resistance, providing a novel strategy to overcome resistance to traditional treatments. Future research should further explore the interaction between key pathways regulating breast cancer autophagy and the immune microenvironment. Additionally, investigating the *in vivo* efficacy of 053 in metastatic lesions and its ability to reverse resistance, as well as verifying whether the combination of 053 with chemotherapy drugs or immune checkpoint inhibitors can improve efficacy, could provide new therapeutic strategies for multi-target intervention in breast cancer. However, the present study has certain limitations as it only examined the autophagy inhibition and immune-promoting effects of compound 053 on breast cancer cells. To further elucidate the mechanistic relationship between 053-induced autophagy inhibition and immunomodulation and to determine whether its immune effects are secondary consequences or independent mechanisms, genetic knockout of key autophagy genes in TNBC cells should be performed.

Acknowledgements

Not applicable.

Funding

The present study was funded by the National Natural Science Foundation of China (grant no. 82374081), Joint Funds for the Innovation of Science and Technology, Fujian Province, China (grant nos. 2023Y9406 and 2021Y9209), Natural Science Foundation of Fujian (grant no. 2024J011065), Major Scientific Research Program for Young and Middle-aged Health Professionals of Fujian Province, China (grant no. 2022ZQNZD008), High-level Talents Training Project of Fujian Cancer Hospital (grant nos. 2022YNG04 and 2023YNG02) and The Fuzhou University Testing Fund of Precious Apparatus (grant no. 2024T019).

Availability of data and materials

The data generated in the present study may be requested from the corresponding author.

Authors' contributions

JL developed the framework of the study; JL,YY, LuC, FC and HZ performed the experiments, investigation and analyzed the data; JL and YY were responsible for drafting the initial manuscript; JL, SC, PQ, YL, LiC and YS interpreted the data and wrote and revised the manuscript; HC and QL designed and supervised the study, interpreted the data and wrote and revised the manuscript; JL, HC and QL confirm the authenticity of all the raw data. All authors read and approved the final version of the manuscript.

Ethics approval and consent to participate

The *in vivo* mouse study procedures were performed in accordance with the regulations of the Laboratory Animal Ethics Committee of the College of Biological Sciences and Engineering, Fuzhou University (Fuzhou, China; approval no. 2022-SG-022). Peripheral blood mononuclear cells were isolated from healthy individuals in compliance with the regulations set forth by the Ethics Committee of Fujian Cancer Hospital (Fuzhou, China; approval no. K2023-305-01). This process included obtaining informed consent documents (approval no. 1.0, 2023.8.18).

Patient consent for publication

Not applicable.

Competing interests

The authors declare that they have no competing interests.

References

1. Sung H, Ferlay J, Siegel RL, Laversanne M, Soerjomataram I, Jemal A and Bray F: Global cancer statistics 2020: GLOBOCAN estimates of incidence and mortality worldwide for 36 cancers in 185 countries. CA Cancer J Clin 71: 209-249, 2021.
2. Xiong X, Zheng LW, Ding Y, Chen YF, Cai YW, Wang LP, Huang L, Liu CC, Shao ZM and Yu KD: Breast cancer: Pathogenesis and treatments. Signal Transduct Target Ther 10: 49, 2025.
3. Obidiro O, Battogtokh G and Akala EO: Triple negative breast cancer treatment options and limitations: Future outlook. Pharmaceutics 15: 1796, 2023.
4. Milane LS, Dolare S, Ren G and Amiji M: Combination organelle mitochondrial endoplasmic reticulum therapy (COMET) for multi-drug resistant breast cancer. J Control Release 363: 435-451, 2023.

5. Liu J, Liu Y, Wang Y, Li C, Xie Y, Klionsky DJ, Kang R and Tang D: TMEM164 is a new determinant of autophagy-dependent ferroptosis. Autophagy 19: 945-956, 2023.
6. Tanida I: Autophagosome formation and molecular mechanism of autophagy. Antioxid Redox Signal 14: 2201-2214, 2011.
7. Quan Y, Lei H, Wahafu W, Liu Y, Ping H and Zhang X: Inhibition of autophagy enhances the anticancer effect of enzalutamide on bladder cancer. Biomed Pharmacother 120: 109490, 2019.
8. Cocco S, Leone A, Piezzo M, Caputo R, Di Lauro V, Di Rella F, Fusco G, Capozzi M, Gioia GD, Budillon A and De Laurentiis M: Targeting autophagy in breast cancer. Int J Mol Sci 21: 7836, 2020.
9. Zhang L, Jiang L, Yu L, Li Q, Tian X, He J, Zeng L, Yang Y, Wang C, Wei Y, *et al*: Inhibition of UBA6 by inosine augments tumour immunogenicity and responses. Nat Commun 13: 5413, 2022.
10. Zhao H, Yang M, Zhao J, Wang J, Zhang Y and Zhang Q: High expression of LC3B is associated with progression and poor outcome in triple-negative breast cancer. Med Oncol 30: 475, 2013.
11. Yu S, Cao Z, Cai F, Yao Y, Chang X, Wang X, Zhuang H and Hua ZC: ADT-OH exhibits anti-metastatic activity on triple-negative breast cancer by combinatorial targeting of autophagy and mitochondrial fission. Cell Death Dis 15: 463, 2024.
12. Hamurcu Z, Delibaşı N, Geçene S, Şener EF, Dönmez-Altuntaş H, Özkul Y, Canatan H and Ozpolat B: Targeting LC3 and Beclin-1 autophagy genes suppresses proliferation, survival, migration and invasion by inhibition of Cyclin-D1 and uPAR/Integrin β1/Src signaling in triple negative breast cancer cells. J Cancer Res Clin Oncol 144: 415-430, 2018.
13. Spinelli FR, Moscarelli E, Ceccarelli F, Miranda F, Perricone C, Truglia S, Garufi C, Massaro L, Morello F, Alessandri C, *et al*: Treating lupus patients with antimalarials: Analysis of safety profile in a single-center cohort. Lupus 27: 1616-1623, 2018.
14. Zheng Z, Liu J, Ma J, Kang R, Liu Z and Yu J: Advances in new targets for immunotherapy of small cell lung cancer. Thorac Cancer 15: 3-14, 2024.
15. Herrera-Quintana L, Vázquez-Lorente H and Plaza-Diaz J: Breast cancer: Extracellular matrix and microbiome interactions. Int J Mol Sci 25: 7226, 2024.
16. Duan Z, Shi Y, Lin Q, Hamaï A, Mehrpour M and Gong C: Autophagy-associated immunogenic modulation and its applications in cancer therapy. Cells 11: 2324, 2022.
17. Galluzzi L, Buqué A, Kepp O, Zitvogel L and Kroemer G: Immunological effects of conventional chemotherapy and targeted anticancer agents. Cancer Cell 28: 690-714, 2015.
18. Xu X, Araki K, Li S, Han JH, Ye L, Tan WG, Konieczny BT, Bruinsma MW, Martinez J, Pearce EL, *et al*: Autophagy is essential for effector CD8(+) T cell survival and memory formation. Nat Immunol 15: 1152-1161, 2014.
19. Liu YC, Shou ST and Chai YF: Immune checkpoints in sepsis: New hopes and challenges. Int Rev Immunol 41: 207-216, 2022.
20. Thomenius MJ, Totman J, Harvey D, Mitchell LH, Riera TV, Cosmopoulos K, Grassian AR, Klaus C, Foley M, Admirand EA, *et al*: Small molecule inhibitors and CRISPR/Cas9 mutagenesis demonstrate that SMYD2 and SMYD3 activity are dispensable for autonomous cancer cell proliferation. PLoS One 13: e0197372, 2018.
21. Eggert E, Hillig RC, Koehr S, Stöckigt D, Weiske J, Barak N, Mowat J, Brumby T, Christ CD, Ter Laak A, *et al*: Discovery and characterization of a highly potent and selective aminopyrazoline-based in vivo probe (BAY-598) for the protein lysine methyltransferase SMYD2. J Med Chem 59: 4578-4600, 2016.
22. Sweis RF, Wang Z, Algire M, Arrowsmith CH, Brown PJ, Chiang GG, Guo J, Jakob CG, Kennedy S, Li F, *et al*: Discovery of A-893, a new cell-active benzoxazinone inhibitor of lysine methyltransferase SMYD2. ACS Med Chemi Lett 6: 695-700, 2015.
23. Zhang B, Liao L, Wu F, Zhang F, Sun Z, Chen H and Luo C: Synthesis and structure-activity relationship studies of LLY-507 analogues as SMYD2 inhibitors. Bioorg Med Chem Lett 30: 127598, 2020.
24. Tam S, Al-Zubaidi Y, Rahman MK, Bourget K, Zhou F and Murray M: The ixabepilone and vandetanib combination shows synergistic activity in docetaxel-resistant MDA-MB-231 breast cancer cells. Pharmacol Rep 74: 998-1010, 2022.
25. Wang K, Zhu X and Yin Y: Maslinic acid enhances docetaxel response in human docetaxel-resistant triple negative breast carcinoma MDA-MB-231 cells via regulating MELK-FoxM1-ABCB1 signaling cascade. Front Pharmacol 11: 835, 2020.
26. Taherian A and Mazoochi T: Different expression of extracellular signal-regulated kinases (ERK) 1/2 and Phospho-Erk Proteins in MBA-MB-231 and MCF-7 cells after chemotherapy with doxorubicin or docetaxel. Iran J Basic Med Sci 15: 669-677, 2012.
27. Jones S, Holmes FA, O'Shaughnessy J, Blum JL, Vukelja SJ, McIntyre KJ, Pippen JE, Bordelon JH, Kirby RL, Sandbach J, *et al*: Docetaxel with cyclophosphamide is associated with an overall survival benefit compared with doxorubicin and cyclophosphamide: 7-year follow-up of US oncology research trial 9735. J Clin Oncol 27: 1177-1183, 2009.
28. Capri G, Tarenzi E, Fulfaro F and Gianni L: The role of taxanes in the treatment of breast cancer. Semin Oncol 23 (Suppl 2): S68-S75, 1996.
29. McLeland CB, Rodriguez J and Stern ST: Autophagy monitoring assay: Qualitative analysis of MAP LC3-I to II conversion by immunoblot. Methods Mol Biol 697: 199-206, 2011.
30. Colosetti P, Puissant A, Robert G, Luciano F, Jacquel A, Gounon P, Cassuto JP and Auberger P: Autophagy is an important event for megakaryocytic differentiation of the chronic myelogenous leukemia K562 cell line. Autophagy 5: 1092-1098, 2009.
31. Mauthe M, Orhon I, Rocchi C, Zhou X, Luhr M, Hijlkema KJ, Coppes RP, Engedal N, Mari M and Reggiori F: Chloroquine inhibits autophagic flux by decreasing autophagosome-lysosome fusion. Autophagy 14: 1435-1455, 2018.
32. Xu Z, Han X, Ou D, Liu T, Li Z, Jiang G, Liu J and Zhang J: Targeting PI3K/AKT/mTOR-mediated autophagy for tumor therapy. Appl Microbiol Biotechnol 104: 575-587, 2020.
33. Cui Y, Shi J, Cui Y, Zhu Z and Zhu W: The relationship between autophagy and PD-L1 and their role in antitumor therapy. Front Immunol 14: 1093558, 2023.
34. Kroczek R and Hamelmann E: T-cell costimulatory molecules: Optimal targets for the treatment of allergic airway disease with monoclonal antibodies. J Allergy Clin Immunol 116: 906-909, 2005.
35. Roy D, Gilmour C, Patnaik S and Wang LL: Combinatorial blockade for cancer immunotherapy: Targeting emerging immune checkpoint receptors. Front Immunol 14: 1264327, 2023.
36. Zhang L, Qiang P, Yu J, Miao Y, Chen Z, Qu J, Zhao Q, Chen Z, Liu Y, Yao X, *et al*: Identification of compound CA-5f as a novel late-stage autophagy inhibitor with potent anti-tumor effect against non-small cell lung cancer. Autophagy 15: 391-406, 2019.
37. Wu ST, Han SS, Xu XM, Sun HJ, Zhou H, Shang K, Liu ZH and Liang SJ: 3-methyladenine ameliorates surgery-induced anxiety-like behaviors in aged mice by inhibiting autophagy-induced excessive oxidative stress. Metab Brain Dis 38: 1913-1923, 2023.
38. Shih FC, Lin CF, Wu YC, Hsu CC, Chen BC, Chang YC, Lin YS, Satria RD, Lin PY and Chen CL: Desmethylclomipramine triggers mitochondrial damage and death in TGF-β-induced mesenchymal type of A549 cells. Life Sci 351: 122817, 2024.
39. Dong X, Zhao R, Li Y, Yu Q, Chen X, Hu X, Ma J, Chen X, Huang S and Chen L: Maduramicin inactivation of Akt impairs autophagic flux leading to accumulated autophagosomes-dependent apoptosis in skeletal myoblast cells. Int J Biochem Cell Biol 114: 105573, 2019.
40. Pan SW, Hu LS, Wang H, Li RT, He YJ, Shang Y, Dai ZL, Chen LX and Xiong W: Resolvin D1 induces mTOR-independent and ATG5-dependent autophagy in BV-2 microglial cells. Curr Med Sci 43: 1096-1106, 2023.
41. Jain V, Singh MP and Amaravadi RK: Recent advances in targeting autophagy in cancer. Trends Pharmacol Sci 44: 290-302, 2023.
42. Liu Q, Yang Y, Cheng M, Cheng F, Chen S, Zheng Q, Sun Y and Chen L: The marine natural product, dicitrinone B, induces apoptosis through autophagy blockade in breast cancer. Int J Mol Med 50: 130, 2022.
43. Young TM, Reyes C, Pasnikowski E, Castanaro C, Wong C, Decker CE, Chiu J, Song H, Wei Y, Bai Y, *et al*: Autophagy protects tumors from T cell-mediated cytotoxicity via inhibition of TNFα-induced apoptosis. Sci Immunol 5: eabb9561, 2020.
44. Prabakaran T, Bodda C, Krapp C, Zhang BC, Christensen MH, Sun C, Reinert L, Cai Y, Jensen SB, Skouboe MK, *et al*: Attenuation of cGAS-STING signaling is mediated by a p62/SQSTM1-dependent autophagy pathway activated by TBK1. EMBO J 37: e97858, 2018.
45. Zhang HJ, Liang CL, Ding XY, Zhang M, Lu SY and Hou L: Manganese-based nano-delivery system for sensitized anti-tumor immunotherapy via combined autophagy inhibition. Chinese Chem Lett 36: 110525, 2025.
46. Herhaus L, Gestal-Mato U, Eapen VV, Mačinković I, Bailey HJ, Prieto-Garcia C, Misra M, Jacomin AC, Ammanath AV, Bagarić I, *et al*: IRGQ-mediated autophagy in MHC class I quality control promotes tumor immune evasion. Cell 187: 7285-7302.e29, 2024.